Optical selection studies of electronic relaxation from the S 1 state of jetcooled anthracene derivatives

Aviv Amirav, Chanan Horwitz, and Joshua Jortner

Citation: The Journal of Chemical Physics **88**, 3092 (1988); doi: 10.1063/1.453953
View online: http://dx.doi.org/10.1063/1.453953
View Table of Contents: http://scitation.aip.org/content/aip/journal/jcp/88/5?ver=pdfcov
Published by the AIP Publishing

Optical selection studies of electronic relaxation from the S_1 state of jet-cooled anthracene derivatives

Aviv Amirav, Chanan Horwitz, and Joshua Jortner
Sackler Faculty of Exact Sciences, School of Chemistry, Tel Aviv University, 69978 Tel Aviv, Israel

(Received 7 April 1987; accepted 7 October 1987)

In this paper we explore the energy dependence of the interstate electronic relaxation rates k_{nr} from the S_1 manifold of anthracene and seven of its isotopic and chemical derivatives, which were inferred from quantum yield data. Absolute fluorescence quantum yields Y from groups of rotational states within the electronic origin $S_1(0)$ and from vibrational states were obtained over the excess energy $E_v = 0$–$3000\ cm^{-1}$ above $S_1(0)$ by the simultaneous interrogation of the fluorescence excitation spectra and of the absorption spectra in seeded, pulsed, planar supersonic jets of Ar. Additional information was obtained from quantum yield data of van der Waals (vdW) complexes of these molecules with Ar. The fluorescence quantum yields from the $S_1(0)$ of anthracene, 9-cyano-anthracene, and 9,10-dibromoanthracene were found to be independent of the rotational state, providing further evidence for the rotational independence of k_{nr} from a single doorway state. From the Y data of the electronic origins and from the E_v dependence of Y we conclude that intersystem crossing (ISC) dynamics of the S_1 manifold is dominated by the interplay between two classes of nonreactive coupling and/or relaxation: (i) Interstate coupling, involving the superposition of direct $S_1 \rightarrow (T_1)$ ISC together with $S_1 \rightarrow (T_x) \rightarrow (T_1)$ mediated ISC through a sparse or dense (T_x) manifold of a higher triplet state; (ii) Intrastate coupling within the S_1 manifold, which sets in with increasing E_v and which results in intramolecular vibrational energy redistribution (IVR) at high E_v. The dominant role of mediated interstate coupling in ISC dynamics from $S_1(0)$ and from low E_v states was inferred from the inverse deuterium isotope effect on the ISC rates, the extreme sensitivity of k_{nr} of deuterated anthracene to a single H atom substitution, and to level shifts induced by complexing with Ar, as well as from the three-orders-of-magnitude difference between the k_{nr} values from the $S_1(0)$ of 9-bromoanthracene and of 9,10-dibromoanthracene. The onset of the mediated ISC is documented by an abrupt drop of Y in the narrow ($E_v = 617$–$805\ cm^{-1}$) energy range for 9,10-dichloroanthracene and by the oscillatory energy dependence of Y vs E_v and the extreme energy sensitivity of Y in the range $E_v = 157$–$800\ cm^{-1}$ of 9,10-dibromoanthracene, which is attributed to near-degeneracies between S_1 states and the mediating (T_x) states. These resonance effects can be drastically modified by dispersive level shifts induced by complexing with Ar. At high excess vibrational energies some universal features of the E_v dependence of k_{nr} are exhibited. These involve a gradual increase of k_{nr} with increasing E_v at medium energies ($E_v = 1000$–$1800\ cm^{-1}$), which correspond to the intermediate level structure for intrastate coupling and a very weak E_v dependence of k_{nr} at high energies ($E_v = 1800$–$3000\ cm^{-1}$), which manifest the effect of statistical intrastate IVR on interstate ISC.

I. INTRODUCTION

The dependence of the interstate radiationless transition rates from photoselected electronically–vibrationally excited states of large collisionless molecules on their excess vibrational energy is central for the elucidation of the processes of intramolecular dynamics. The pioneering work of Schlag and van Weyssenhoff,[1] Parmenter,[2] Rice,[3] Lim,[4] and their colleagues focused on optical selection studies of interstate radiationless transitions in the low-pressure gas phase. The information stemming from bulb experiments was intrinsically limited due to thermal inhomogeneous broadening effects, e.g., rotational broadening and vibrational congestion, which precludes photoselective vibrational excitation. Photoselection of well-characterized rotational–vibrational electronically excited states of large "isolated" molecules can be accomplished in seeded supersonic expansions.[5,6] Basic information on optical selection in interstate radiationless decay from the S_1 manifold of large molecules has emerged recently from time-resolved spectroscopy in jets.[6–23] Supplementary and complementary information can be obtained from energy-resolved observables, e.g., fluorescence quantum yields. Relative fluorescence quantum yields from different groups of rotational states in the S_1 electronic–vibrational origin of jet-cooled aniline was explored by Amirav *et al.*[24] Relative fluorescence quantum yields from photoselected vibrational states in the S_1 manifold of jet-cooled large molecules were reported by Levy *et al.*[25] for transstilbene and by us for 9,10-dichloroanthracene[26] and transstilbene.[26] Subsequently, we have measured[27] the absolute fluorescence quantum yields from the vibrationless electronic origin $S_1(0)$ of several aromatic molecules and their derivatives. Recently, we have extended the experimental methodology to obtain quite extensive information on the excess vibrational energy dependence of the absolute fluorescence quantum yields from photoselect-

 0021-9606/88/053092-19$02.10

ed vibrationally excited states in the S_1 manifold on a variety of jet-cooled large aromatic molecules.[28–31] These studies have provided information on both nonreactive electronic relaxation and on reactive photochemistry in isolated large molecules.

In this paper we focus on optical selection studies of nonradiative electronic relaxation from the S_1 manifold of anthracene and some of its derivatives, i.e., anthracene-D_{10}, anthracene-D_9H, 9-methylanthracene (9MeA), 9-cyanoanthracene (9CNA), 9,10-dichloroanthracene (9,10DCA), 9,10-dibromoanthracene (9,10DBA), and 9-bromoanthracene (9BA), as well as some of their van der Waals (vdW) complexes with Ar. We report on the dependence of the absolute fluorescence quantum yields Y from photoselected vibrational states on the excess vibrational energy E_v above the S_1 electronic origin of these jet-cooled molecules and complexes. The absolute fluorescence quantum yields were determined from the simultaneous interrogation of the fluorescence excitation spectra and the absorption spectra of these molecules in seeded, pulsed, planar, supersonic jets,[24,26–30] using a pulsed xenon lamp and a monochromator and adopting the calibration method previously advanced by us.[27] The refinement of our experimental techniques allows for the accurate determination of absolute fluorescence quantum yields in the range $1–10^{-4}$. Accordingly, our experimental approach can provide information on fast intramolecular relaxation times from photoselected internal states on the ~ 1 ps time domain. The information emerging from our study of electronic relaxation from the S_1 manifold of jet-cooled anthracene, its derivatives, and some vdW complexes can be summarized as follows:

(1) Mediated intersystem crossing. Electronic relaxation from the S_1 electronic manifold of these molecules proceeds via S_1–T_1 intersystem crossing (ISC), which is mediated by a higher triplet (T_x) state.[32–45] While the occurrence of the S_1–T_x–(T_1) mechanism in condensed phases has been documented previously on the basis of the temperature dependence of ISC, energetic data, and the buildup times of triplet–triplet absorption,[32–45] the present results provide new information on the energetic spread of the T_x states and their role in mediating the radiationless decay of specific vibronic levels in the S_1 manifold of this class of molecules under collisionless conditions.

(2) The onset of mediated intersystem crossing. A "step-like" dependence of the fluorescence quantum yield vs the excess vibrational energy, which is manifested by an abrupt drop of Y in a narrow range of E_v, is exhibited in certain compounds, e.g., 9,10DCA and is attributed to the onset of the mediated intersystem crossing.

(3) The control of electronic relaxation by microscopic solvent effects on the molecular energy levels. The dispersive stabilization of the S_1 state by vdW complexing with rare-gas atoms[47] provides a novel approach for the exploration of the remarkable quantitative modification of ISC dynamics, which is induced by small level shifts of the S_1 levels relative to the mediating T_x states.

(4) Resonance effects. A strong oscillatory dependence of Y vs E_v for 9,10DBA presumably manifests novel resonance effects of the mediating states on intersystem crossing. A preliminary report of this effect was presented.[48]

(5) The role of vibrational energy redistribution (IVR) on electronic relaxation. Intersystem crossing at high vibrational excitation of the S_1 manifold exhibits a universal trend of weak energy dependence of the lifetimes on E_v, manifesting the consequences of intrastate IVR on interstate electronic relaxation.

II. EXPERIMENTAL

A scheme of the experimental setup is shown in Fig. 1. A pulsed linear nozzle slit (Fig. 2) generated a pulsed planar jet of the large molecule seeded in Ar. The pulsed nozzle triggered a pulsed lamp through a variable delay unit, achieving temporal matching of the light and gas pulses. The light pulse was focused onto the entrance slit of the monochromator and then refocused parallel to the long axis of the linear nozzle. The light was detected both before and after crossing the supersonic expansion and the difference was monitored by a differential amplifier, resulting in the absorption signal which was normalized to the incident intensity. The fluorescence was focused and detected in a perpendicular direction to both the light pulse and the gas pulse propagation directions. All the signals, i.e., the fluorescence excitation, the absorption, and the reference light intensity were simultaneously detected and electronically processed using a triple-gated amplifier, a voltage divider, and a double pen recorder. The absorption and fluorescence spectra, both being normalized to the incident light intensity, were simultaneously recorded. In what follows, the components of the system will be described.

A. Vacuum system

The pumping system consisted of a 4 in. diffusion pump (Varian VHS 4) and two mechanical pumps (Edwards)

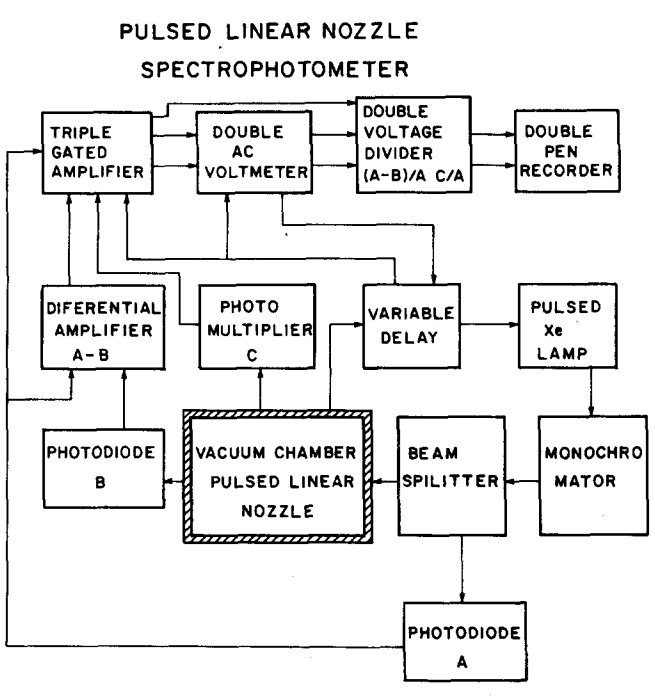

FIG. 1. Experimental setup for the measurement of absorption fluorescence excitation and quantum yields in seeded, pulsed planar supersonic expansions.

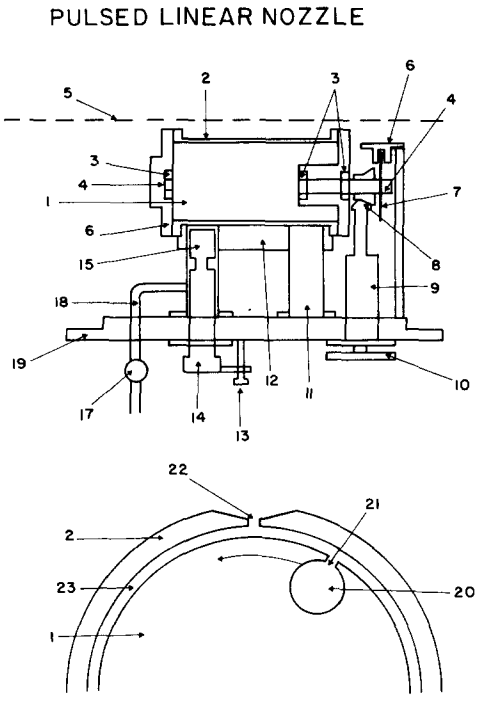

FIG. 2. A schematic diagram of the pulsed linear nozzle source. (1) rotating cylinder, (2) stator, (3) two flanges with ball bearings, (4) axle, (5) direction of light pulses, (6) optical switch serving for triggering of light pulses, (7) slotted disk, (8) two conical gears, (9) ferrofluid rotatory vacuum feedthrough, (10) motor pulley, (11) mechanical support, (12) heating and cooling block, (13) adjusting screw for sample compartment, (14) sample compartment handle, (15) sample compartment, (16) flange-stator sealing (metal to metal), (17) gas valve, (18) gas tube, (19) mounting flange, (20) gas reservoir, (21) linear slit in the rotor, (22) linear slit in the stator, (23) 25 μ tolerance between stator and rotor (lubricated).

with pumping speeds of 200 ℓ/min and 350 ℓ/min. The vacuum system contained a baffled entrance and exit CaF_2 windows. A quartz lens (51 mm focal length and diameter) served for the collection of the fluorescence light and also acted as a vacuum window. The pulsed nozzle and a liquid N_2 cold trap were located in the two main flanges of the vacuum chamber.

B. Pulsed linear nozzle

The pulsed linear nozzle, which is described in Fig. 2, constitutes a refined version of the linear nozzle developed in this laboratory.[24] This mechanically operated device has a rotating cylinder with a gas mixture reservoir and the gas mixture was expanded through a linear slit. A rotating cylinder (rotor) with a slit was spun inside a fixed stator, which also had a slit. Two linear nozzles were used with slit dimensions of 0.32×90 mm and of 0.22×35 mm. The temporal overlap of the rotor's and stator's slits allows for the expansion of the gas mixture into the vacuum chamber, resulting in the formation of the pulsed planar jet. The rotor was mounted on two flanges with ball bearings and the axle was driven by two conical gears, one of which was mounted on a ferrofluid rotatory vacuum feedthrough. The rotor was rotated by an a.c. motor, which was coupled to the rotor by an O-ring belt connection. The diameter of the rotor slit was 50 mm, with a tolerance of 20–30 μ. The nozzle could be heated (cooled) using a heating (cooling) block. The sample compartment can be detached and taken out of the evacuated nozzle by swinging the compartment handle, and its temperature could be adjusted by using a screw which could change its distance from the heating block. The nozzle could be operated in the temperature range up to 220 °C. Ar gas in the pressure range $p = 50$–200 Torr that was fed from a valve and a tube through the sample compartment chamber and subsequently passed to the gas reservoir through a groove. The backing pressure was controlled using a needle valve and a manometer (not shown in Fig. 2). A slotted disk and an infrared optical switch (Spectronix 1874) served for the triggering of the pulsed lamp.

The nozzle was operated at a frequency of 5–13 Hz, resulting in 150–350 μs, gas pulses. This pulsed linear nozzle constitutes a reliable device, which was routinely operated for periods exceeding 24 h. The device could be operated for several months before a mechanical failure would be encountered or a lubrication service required.

C. Light source

We have used a short-arc xenon lamp (Osram XBO 75 w/2), which was ignited and simmered at 3–5 A, utilizing Oriel's universal power supply. The simmered lamp was pulsed using a 45 μF capacitor charged to 100–200 V in conjunction with a capacitor charger.[49] This mode of operation results in the increase of the brightness of the lamp by about three orders of magnitude, as compared to the conventionally operated lamp. The intensity of the pulsed simmered lamp measured at the monochromator exit slit at 0.4 Å resolution was 10^{-10} J. The stability of individual pulses (pulse duration 24 μs) was about 1%, and after comparison with the reference signals the noise was found to be better than 0.1% for a single pulse.

D. Optics and detectors

The pulsed light beam was focused with a single 1 in. lens (1 in. focal length) onto the entrance slit of a monochromator. Two monochromators were used:

(1) A 0.3 m McPherson 218 monochromator equipped with a grating of 2400 lines/mm. The spectral resolution attained with slits of 30 μ was 0.4 Å (2.8 cm^{-1} at 3700 Å).

(2) A 0.75 m/spex monochromator equipped with a 2400 lines/mm grating. The spectral resolution was 0.11 Å for 15 μ slits (0.8 cm^{-1} at 3700 Å). The spectral resolution attained at slits of 6 μ (as determined by the splitting of the Hg lines) was 0.06 Å. Typical resolutions routinely used in our work were in the range 0.06–0.6 Å (0.4 $cm^{-1}-4$ cm^{-1}).

The light from the monochromator was split by a beam splitter, consisting of a partially mirrored CaF_2 window or a pair of sapphire windows for reference light detection. The beam from the monochromator before passing through the beam splitter was focused using a 1 in. lens (4 in. focal length) parallel to the long axis of the slit nozzle at a distances of $x = 6$–16 mm from the slit. Both the direct and the reference pulsed light beams were detected with vacuum

photodiodes (Hammamatsu R645 or R727). The fluorescence was detected using a photomultiplier (Hammamatsu R269).

E. Electronics and data processing

All the techniques employed in this work were homemade. The reference signal I_0 and the direct transmission signal I were fed to a differential amplifier with adjustable relative gain for zeroing in the absence of absorption. The relative absorption signal $(I_0 - I)$, obtained from the differential amplifier, the fluorescence signal I_F and the reference signal, I_0, were simultaneously processed using a triple-gated amplifier. In order to correct the chromaticity of the beam splitter and to obtain a flat absorption baseline, we have used a double ac voltmeter which is connected with the variable delay unit. This piece of electronics doubled the number of light pulses relative to the number of gas pulses. In this setup the difference signal $(I_0 - I)$ and the fluorescence signal were simultaneously measured by the gate amplifier with a single pulse gating. These signals were sent to the double ac voltmeter which measured the difference between the synchronized and unsynchronized signal pulses. The reference signal I_0 was measured by the gated amplifier and used for normalization using a voltage divider. Such an on-line comparison between I and I_0 was corrected for absorption baseline spectral drifts. The proper timing of the gas pulse and of the light pulse was achieved by using a variable delay unit, which could be operated in the range 10 μs–10 ms.

F. Data recording

The absorption $(I_0 - I)/I_0$ and the normalized fluorescence I_F/I_0 were simultaneously recorded using a double pen recorder. Absorption spectra and fluorescence excitation (LMIF) lamp-induced fluorescence spectra were recorded. Accurate quantum yield data were obtained by recording the fluorescence excitation and the absorption at a fixed wavelength, increasing the time constant to obtain a high precision, while the baseline was recorded with a delay of 10 ms. In addition, quantum yield data were obtained in a narrow spectral range and with a high time constant to correct for the small contribution of dimers to the absorption spectrum and to the fluorescence background.

Absolute quantum yields Y were determined using the calibration scheme previously developed by us,[27] which rests on the simultaneous measurements of relative quantum yields from the electronic origins of a pair of molecules in a binary doped supersonic expansion, and the assignment of a value of $Y = 1$ to fluorescence from the electronic origins of transstilbene and of 9,10DCA.[27] Absolute fluorescence quantum yields in the range $Y = 1 - 10^{-4}$ could be routinely recorded. The uncertainty of the Y data was estimated to be 2% for intense spectra features, while for weak spectral features the accuracy was 10%.

G. Chemicals

All the chemicals used by us were commerically purchased. Care must be taken to ensure the purity of those materials, whose consituent molecules exhibit a low fluorescence quantum yield in the jet. In such a system, a minor amount of an impurity with a high Y will exhibit a spurious fluorescence signal. A typical example for a trace of impurity fluorescence is provided in Fig. 3, where we portray a portion of the fluorescence excitation and the absorption spectra of 9-bromoanthracene, whose electronic origin at 3742 Å is characterized by $Y = 0.0024$. The intense spectral feature in the fluorescence excitation at 3610.2 Å, which is masked by the noise in the absorption spectrum, corresponds to the electronic origin of the anthracene molecule ($Y = 0.67$). The anthracene molecule, which is present as an impurity in 9BA at a concentration of about 1%, provides the dominant spectral feature in the fluorescence excitation spectrum, but is buried within the noise in the absorption spectrum of the low-Y 9BA.

III. RESULTS AND DISCCUSION

A. Rotational structure of the electronic origin

A partial resolution of the rotational contour of the electronic origin of the first spin-allowed $^1S_0 \rightarrow {}^1S_1$ electronic transition of anthracene-H_{10}, anthracene-D_9H, and anthracene-D_{10} could be accomplished under our experimental conditions of 0.5–1 cm^{-1} spectral resolution. Figure 4 shows the characteristic B-type (perpendicular) rotational contours of the three isotopic molecules, obtained by LMIF and absorption spectroscopy. These experimental results are in

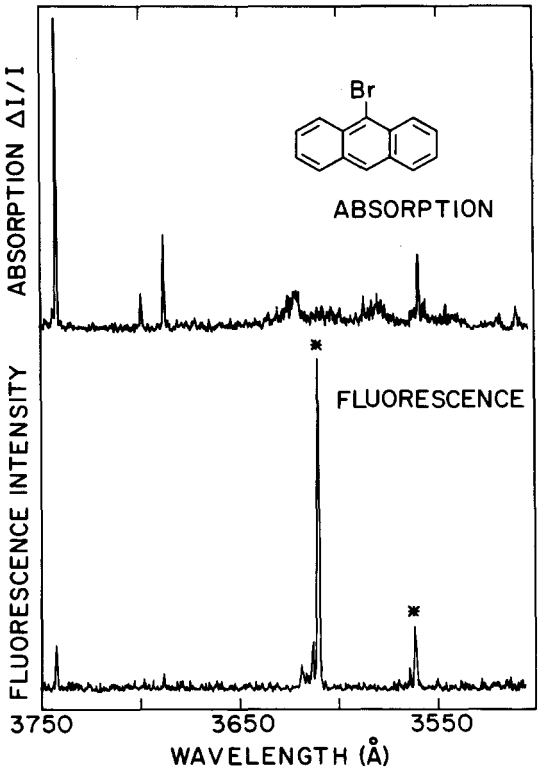

FIG. 3. Absorption spectrum (top curve) and fluorescence excitation spectrum (lower curve) over the range 3750–3550 Å of 9BA in a pulsed planar jet of Ar. Stagnation pressure $p = 110$ Torr and nozzle temperature $T = 140$ °C. Distance from nozzle $X = 10$ mm. The intense feature at 3610 Å in the fluorescence excitation spectrum is due to anthracene impurity.

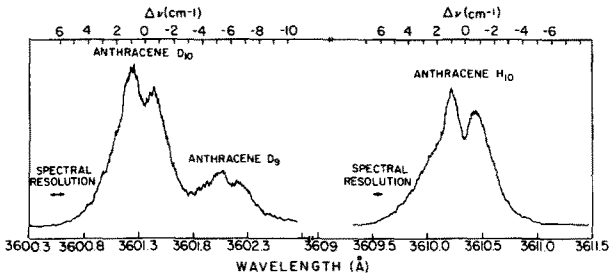

FIG. 4. Fluorescence excitation spectra of the electronic origins of anthracene-H_{10}, anthracene-D_9H, and anthracene-D_{10} in a pulsed planar jet of Ar $p = 100$ Torr, $T = 140$ °C, $X = 10$ mm. The spectral resolution is marked on the figure.

accord with recent LIF jet spectra of anthracene[18] and with the well-established theoretical assignment of this electronic transition to the short axis polarized $^1A_{1g} \rightarrow {}^1B_{2u}$ excitation.[50] An analysis of the rotational contours of anthracene was previously performed,[18] assuming that the rotational constants are invariant upon electronic excitation. We have conducted numerical simulations of the rotational contours of anthracene, accounting for the (small) changes in the rotational constants. The rotational constants for the two combining states (Table I) were calculated using the Ross–McHough recipe.[51] These were derived from the molecular structures of the $^1A_{1g}$ and $^1B_{2u}$ states, being based on the bond-length–bond-order relations using Pariser's wave functions.[50] The ground state rotational constants are close to those inferred by Lambert *et al.*[18] from structural data. The numerical simulations were conducted using the asymmetric rotor program of Birss and Ramsay.[52] The range of J values was taken from $J = 0$ to $3J$ max, where J max corresponds to the most populated J value at a given temperature. The K values were taken in the range $K = 0$–50. Convolution of the experimental spectral resolution was performed by assigning a width of 0.5 cm^{-1} to each line. Typical results for simulations in the temperature range $T = 2$–40 K are presented in Fig. 5. Regarding the accuracy of the excited-state rotational constants, we have found that at low temperatures, which are of interest to us, small changes ($\sim 1\%$) in A', B', and C' result in negligible changes in the energetic parameters of the low-temperature rotational contours and in quite a marked change in the intensity distribution within the contour (Fig. 6). The experimental data for the intensity ratio between the maxima of the P and R branches favor the values of ΔA, ΔB, and ΔC of Table I over the first-order intelligent guess[18] $\Delta A = \Delta B = \Delta C = 0$. Figure 7 shows the comparison between the experimental LMIF spectrum of the S_1 origin of anthracene-H_{10} and the "best fit" of the simulated spectrum. A typical rotational temperature of this large molecule in the planar jet is $T_R = 20$ K under our experimental conditions. This relatively high rotational temperature is a consequence of the short-interrogation distance $X = 10$ mm from the nozzle, the high relative concentration (up to $\sim 1\%$) of the large molecule in the expansion, and the large cross section (1×4 mm) of the interrogating light beam.

TABLE I. Rotational constants for anthracene (in cm^{-1}).

State	A	B	C
S_0	0.071 70	0.015 12	0.012 49
S_1	0.071 82	0.015 00	0.012 40

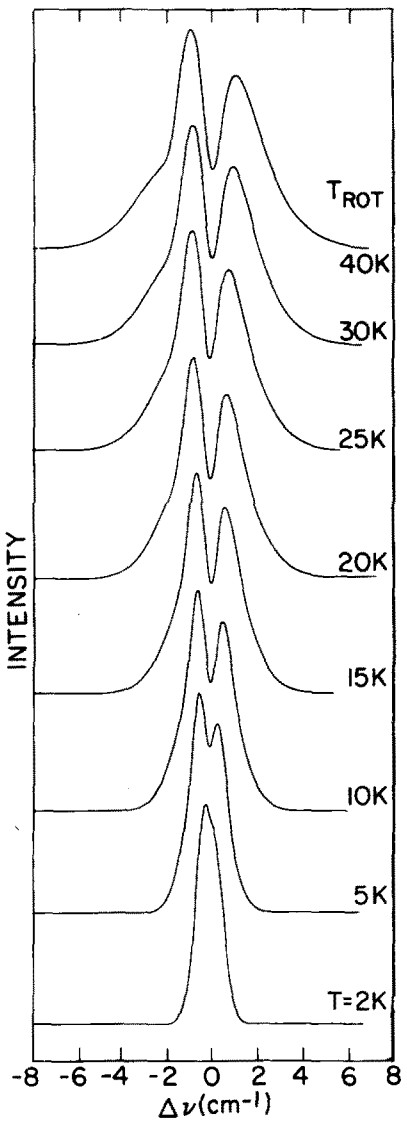

FIG. 5. Numerical simulations of the temperature dependence of the rotational contours for the 0–0 band of anthracene for rotational temperatures $T_{rot} = 2$–40 K. Rotational constants from Table I. Spectral resolution 0.5 cm^{-1}.

B. Fluorescence quantum yield from the electronic origin

The fluorescence quantum yield for the S_1 electronic origin was found to be independent of the rotational state. Excitation of groups of rotational states within a spectral width of 0.5 cm^{-1} within the low energy P branch (which also contain a contribution from the Q branch) and from the high energy R branch revealed that the absolute quantum yield is independent of the rotational quantum numbers $J'K'$ (Fig. 8). Similar results were obtained for Y from the electronic origin of 9,10DBA ($Y = 0.72$) and of 9CNA

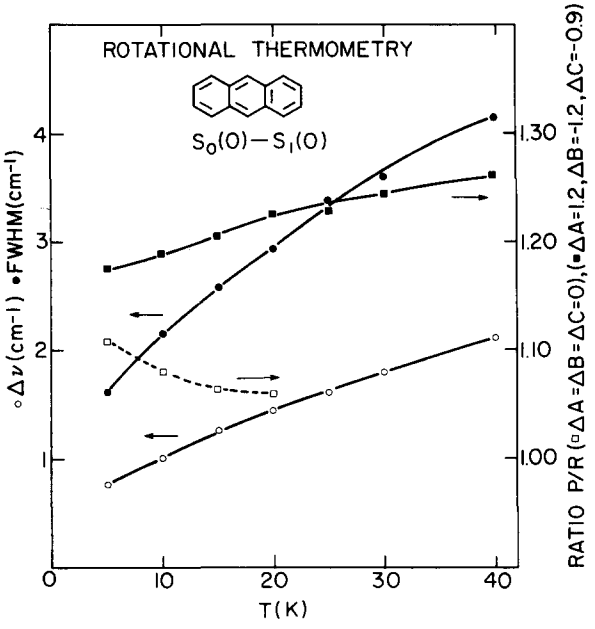

FIG. 6. The rotational temperature dependence of the separation ($\Delta\nu$) of the $P(+Q)$ and R branches, the width of the rotational contour at 50% intensity point (FWHM) and the intensity ratio between the maxima of the P and R branches (ratio P/R) for the electronic origin of anthracene. The P/R ratio is very sensitive to the changes in the rotational constants between the two electronic states. □ P/R ratio for $\Delta A=\Delta B=\Delta C=0$; ■ P/R ratio for the data of Table I, with the values of ΔA, ΔB, and ΔC being given in units of 10^{-4} cm^{-1}.

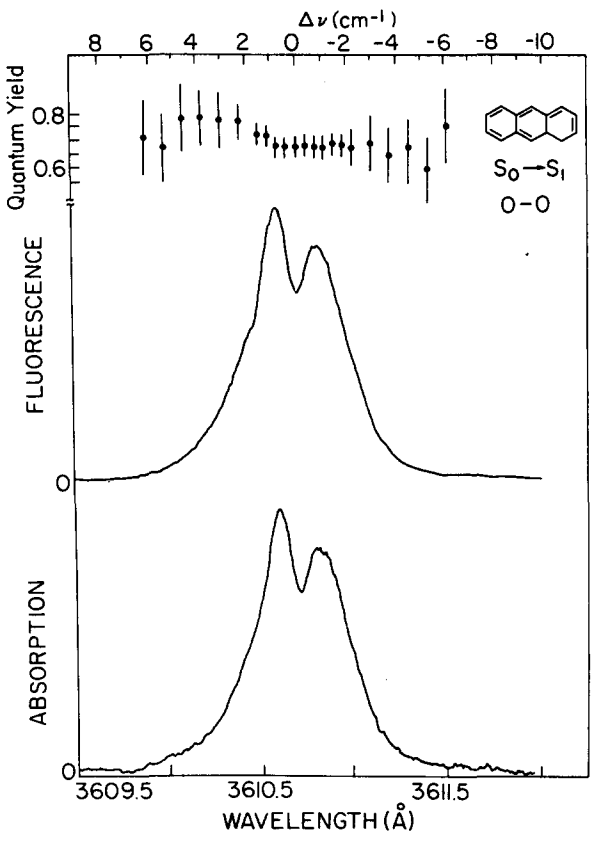

FIG. 8. Absorption spectrum, fluorescence excitation spectrum, and absolute fluorescence quantum yields from the $S_0\rightarrow S_1$ electronic origin of anthracene. $P=110$ Torr, $T=140$ °C, $X=6$ mm, spectral resolution 0.6 cm^{-1}.

($Y=1.0$). The dominant nonradiative decay channel for the $S_1(0)$ electronic origin involves interstate electronic relaxation, which is due to S_1-triplet intersystem crossing (ISC) with the final triplet dissipative channel corresponding to the statistical limit. The invariance of the fluorescence quantum yield to the group of rotational states provides additional evidence that electronic relaxation in the statistical limit is invariant with respect to the rotational state. This result is supported by previous experimental work on the rotational independence of electronic relaxation from the S_1 electronic origin of aniline,[24] of tetracene,[8] and of the rotational state independence of ISC of single rovibronic levels in the S_1 manifold of benzene,[54(c)] and with theoretical calculations.[53] Four remarks regarding the rotational state independence of nonreactive intramolecular radiationless processes are in order:

(1) The rotational independence of the electronic relaxation observed herein pertains to the decay of an "isolated" doorway state, i.e., the electronic origin which is coupled by $J'K'$ independent, that is, spin–orbit interaction V to a "statistical" background manifold. In this case the decay rate $\Delta=2\pi V^2\rho$ and the quantum yield $Y=\Gamma_r/(\Gamma_r+\Delta)$, with Γ_r being the radiative width of the doorway state, are independent of $J'K'$.[53]

(2) At higher vibrational energies of the S_1 manifold when Coriolis coupling between S_1 vibrations prevails, the fluorescence quantum yield may be dependent of $J'K'$.[54–56]

(3) In the intermediate level structure, for interstate coupling, where the doorway state is coupled to a sparse background manifold, the quantum yield is $Y\sim\Gamma_r/N\langle\gamma\rangle$, with $\langle\gamma\rangle$ being an (average) decay width of the background states and N is the dilution factor.[29] The breaking of K selection rules for interstate coupling may result in the dependence of N on J', leading to the dependence of the quantum yield on J'. In this case the rotational dependence of the quantum yield originates from the J' dependent dilution of the radiative lifetime.[29]

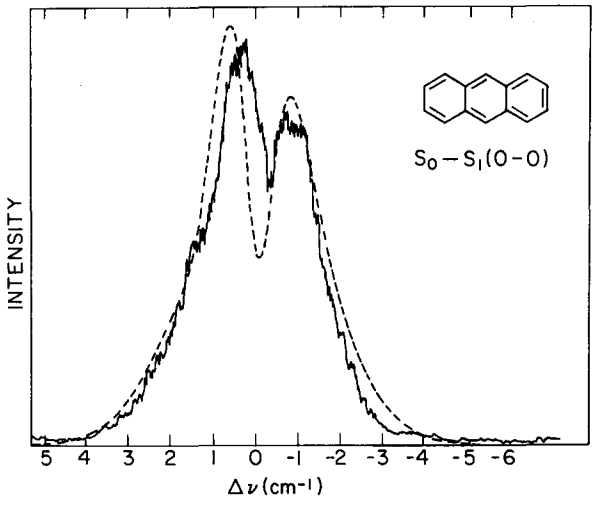

FIG. 7. A comparison between the experimental spectrum of the electronic origin of anthracene in a planar supersonic jet $P=110$ Torr, $T=130$ °C, $X=10$ mm, spectral resolution 0.5 cm^{-1} (solid curve) with the numerical simulation of the rotational contour at $T_{rot}=20$ K.

(4) The intermediate level structure may prevail for either interstate or intrastate coupling with K selective Coriolis coupling between the background states whereupon Y will become rotational state dependent.[57]

The present situation for the decay of S_1 origin corresponds to case (1).

C. Quantum yields from electronic origins of anthracene and some of its isotopic derivatives

A large inverse deuterium isotope effect for electronic relaxation, i.e., intersystem crossing (ISC) from the $S_1(0)$ electronic origin of jet-cooled anthracene-H_{10} and anthracene-D_{10} was inferred from quantum yield data[28] and confirmed by decay lifetime measurements.[19,22] We have measured the absolute fluorescence quantum yields at the $S_1(0)$ electronic origin of anthracene-H_{10}, anthracene-D_9H and anthracene-D_{10}, all of which were interrogated at the dip of the B-type rotational contour. A preliminary report of the Y data between the R and the $P(+Q)$ branches for anthracene-H_{10} and anthracene-D_{10} has been provided.[28] In Table II we present these Y data together with the lifetime, τ, data of Schlag,[23] Lim,[22] and Zewail,[19] which result in the pure radiative lifetime τ_{rad} and the ISC rates k_{nr}. From these results the following is apparent:

(1) The pure radiative lifetimes are invariant with respect to isotopic substitution, as expected.

(2) A very large inverse deuterium isotope effect, i.e., $k_{nr}(D_{10})/k_{nr}(H_{10}) \simeq 15$, is exhibited on the ISC rate from the $S_1(0)$ origin of anthracene-D_{10} relative to that of anthracene-H_{10}.

(3) A dramatic decrease of the ISC rate from the $S_1(0)$ origin, i.e., $k_{nr}(D_9H)/k_{nr}(D_{10}) \simeq 1/7$, is induced by a single H atom substitution.

It has been pointed out[22,28] that the huge inverse deuterium isotope effect on the $S_1 \rightarrow T_1$ ISC from the $S_1(0)$ state cannot be accounted for in terms of the conventional arguments based on the role of Franck–Condon factors in interstate coupling, rather this effect was attributed to ISC, which is mediated by a manifold of (T_x^k) triplet vibronic levels and which corresponds to a higher triplet state. The relevant coupling scheme is

$$|S_1\rangle \xrightarrow{V_{so}} \{|T_x^k\rangle\} \xrightarrow{V_{vib}} \{|T_1\rangle\}, \tag{1}$$

where V_{so} and V_{vib} represent spin–orbit and vibronic coupling, respectively. The $\{|T_x^k\rangle\}$ manifold in the vicinity of $S_1(0)$ is assumed to be sparse, whereupon the $|S_1\rangle \rightarrow \{|T_x^k\rangle\}$ coupling for all k states correspond to an off-resonant situation. Under these circumstances the nonradiative decay rate of $|S_1\rangle$ is given by the second-order contribution[28]

$$\gamma_{II}(S_1) = \sum_k |V_{so}^{(k)}|^2 \Delta_k / \{[E(S_1) - E(T_x^k)]^2 + (1/2\Delta_k)^2\}, \tag{2}$$

where $V_{so}^{(k)} = \langle S_1|V_{so}|T_x^k\rangle$ represents spin–orbit coupling between the zero-point vibrational level of S_1 and a vibrational level k in the sparse T_x manifold, while $\Delta_k = 2\pi|\langle T_x^k|V_{vib}|T_1\rangle|^2\rho$ is the decay width of the $|T_x^k\rangle$ state due to its internal conversion to the dense statistical $\{|T_1\rangle\}$ manifold. The ISC rate, Eq. (2), contains a cumulative contribution for several mediating states. Both the widths Δ_k and the spin–orbit coupling terms are expected to exhibit a small normal deuterium isotope effect. The large inverse deuterium isotope effect was attributed[22,28] to the sensitivity of the energy defects $|E(S_1) - E(T_x^k)|$, which appear in Eq. (2), on the isotopic substitution. The following implications of this result are apparent:

(A) Inverse deuterium isotope effect on $\gamma_{II}(S_1)$. Since the $\{|T_x^k\rangle\}$ vibrational manifold is more dense in the vicinity of $S_1(0)$ of anthracene-D_{10} than of anthracene-H_{10}, some of the energy defects $|E(S_1(0) - E(T_x^k)|$ are expected to be smaller for deuterated anthracenes, resulting in the enhancement of γ_{II}.

(B) Level structure sensitivity of γ_{II}. The remarkable decrease of k_{nr} by a single H atom substitution (Table II) together with the irregular dependence of k_{nr} on the isotopic substitution (Table II) manifest the crucial role of energetic shifts of the mediating state. A single H atom substitution of perdeuteroanthracene results in the following effects: (i) A change in the level structure of the $\{|T_x^k\rangle\}$ manifold, which results in energetic shifts of the mediating states relative to $S_1(0)$. (ii) An energetic shift of the $S_1(0)$ origin. According-

TABLE II. Quantum yields from the S_1 electronic origins of anthracene and its deuterated derivatives.

Molecule	$(cm^{-1})^a$	Y^b	$\tau_{rad}k_{nr}{}^c$	τ (ns)$^{d-g}$	τ_{rad} (ns)^h	k_{nr} (s^{-1})
Anthracene-H_{10}	0	0.67	0.49	4.0[d] 4.4[e]	32 ± 3	0.15×10^8
Anthracene-D_9H	7	0.49	1.04	17[d]	34 ± 3	0.31×10^8
Anthracene-D_{10}	69	0.134	6.69	18[d] 21.5[e] 20[f] 18[g]	30 ± 3	2.23×10^8

[a]Spectral shifts of electronic origin relative to that of anthracene-H_{10}.
[b]Absolute quantum yields. Present work.
[c]Calculated from $\tau_{rad}k_{nr} = (Y^{-1} - 1)$
[d]Reference 22.
[e]Reference 19.
[f]Reference 23.
[g]A. Amirav and J. Jortner (unpublished).
[h]Calculated from $\tau_{rad} = Y^{-1}\tau$.

ly, the energetic defects $|E(S_1(0) - E(T_x^k)|$ are modified, resulting in a marked change in γ_{II}. This level structure sensitivity manifests near-resonance effects of the mediating states on the ISC rate. In the rationalization of the surprising inverse deuterium isotope effect and level structure sensitivity of $S_1(0)$ for the isotopic species of anthracene, the role of level shifts originating from effects (i) and (ii) cannot be disentangled. This can be accomplished by the exploration of fluorescence quantum yields from vdW complexes of deuterated anthracenes with Ar, which leaves the $\{|T_x^k\rangle\}$ manifold practically invariant, and result in an energetic shift of the $S_1(0)$ origin relative to the $\{|T_x^k\rangle\}$ states.

D. Erosion of the inverse deuterium isotope effect by complexing with Ar

The formation of vdW molecules consisting of large aromatic molecules bound to rare-gas atoms is well documented.[47] The exploration of microscopic solvation effects on the spectral shifts of aromatic, rare-gas vdW complexes has resulted in extensive information on the energetics of the $S_1(0)$ electronic origin, relative to the vibrationless ground state. For heavy rare-gas atoms, i.e., Ar, Kr, and Xe these red spectral shifts are dominated by dispersive interactions, resulting in the lowering of the energy of the $S_1(0)$ state of the complex relative to that of the bare molecules. A typical example is provided in Fig. 9 which portrays the LMIF spectra of anthracene–Ar_n being in accord with previous data,[58] and of perdeuterated anthracene–Ar_n, which reveal the gradual red shifts of these complexes, with increasing coordination number. The dominating contribution of these red shifts originates from dispersive interactions, which are considerably larger for the $S_1(0)$ state than for the states in the $\{|T_x^k\rangle\}$ manifold. Provided that an anthracene molecule is complexed with an "inert" ligand, which does not modify the intramolecular spin–orbit coupling interaction, one expects a dramatic modification of the mediated nonradiative ISC rate from $S_1(0)$ due to the modification of the energy defects $|E[S_1(0)] - E(T_x^k)|$ in Eq. (2). This expectation is born out by the measurements of the quantum yields from the electronic origins of the vdW complexes of anthracene Ar_1 and perdeuteroanthracene Ar_1, where the Ar atom constitutes nearly an inert ligand, which does not exhibit an external heavy atom effect on ISC. In Fig. 10 we present the absorption and LMIF spectra of the bare isotopic molecules and their complexes with Ar, being labeled as the bare isotopic molecules and their complexes with Ar, which are labeled as $n = 1$. The absolute quantum yields result in the

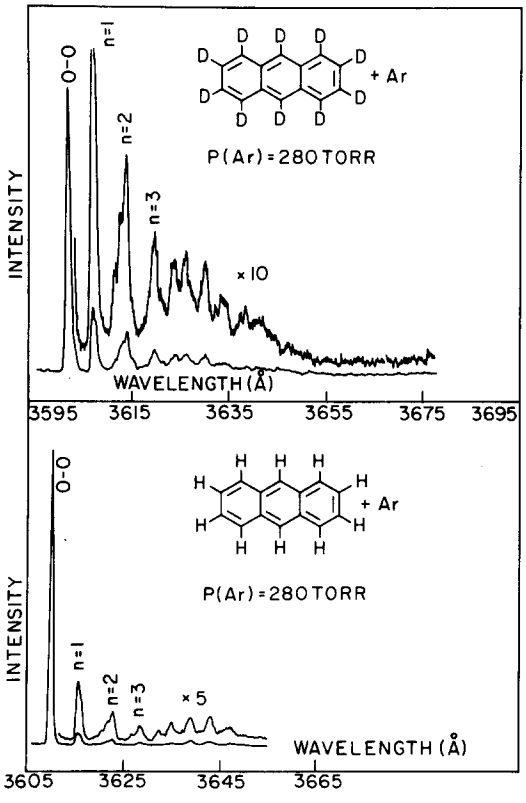

FIG. 9. Fluorescence excitation spectra in the range 3600–3670 Å of anthracene-D_{10} and anthracene-H_{10} at high stagnation pressure of Ar $P = 280$ Torr. The electronic origins of the bare molecules are marked 0–0. The spectral features of the electronic origins of anthracene Ar_n and of anthracene-D_{10} Ar_n are exhibited towards lower energies of the bare molecules electronic origin. The coordination number n of the complexes, assigned on the basis of the order of appearance of these features, is marked on the spectra.

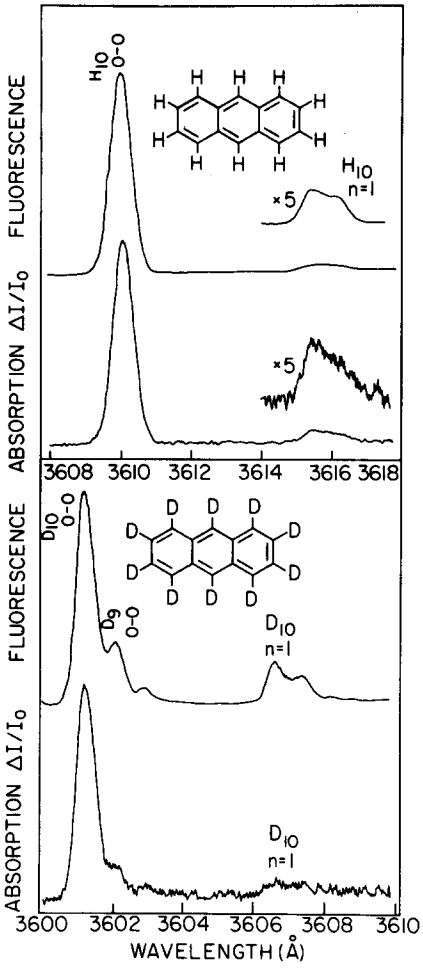

FIG. 10. Absorption spectra and fluorescence excitation spectra of anthracene and anthracene-D_{10} in the spectral range 3600–3610 Å at high stagnation pressure of Ar $P = 220$ Torr for anthracene-H_{10} and $P = 160$ Torr for anthracene-D_{10}. $T = 136$ °C, and $X = 6$ mm. The electronic origins of the bare molecules are marked 0–0. The electronic origins of the anthracene Ar and of anthracene-D_{10} Ar complexes are marked by H_{10} $n = 1$ and D_{10} $n = 1$, respectively.

product of the nonradiative rate and the pure radiative lifetime.

$$k_{nr}\tau_{\rm rad} = Y^{-1} - 1. \quad (3)$$

The values of $k_{nr}\tau_{\rm rad}$ (Table III) reveal a dramatic decrease of the k_{nr} value for perdeuterated anthracene–Ar_1 relative to that of the bare molecule. Furthermore, the values of $k_{nr}\tau_{\rm rad}$ for the Ar complexes of perdeuteroanthracene and of anthracene are practically identical, exhibiting the erosion of the large inverse deuterium isotope effect on ISC due to the modest shift of the $S_1(0)$ state by -43 cm^{-1}. We note in passing that the twofold increase of the values of $k_{nr}\tau_{\rm rad}$ for anthracene. Ar_1 relative to that of bare anthracene can originate from these causes: (i) The modification of the pure radiative lifetimes by complexing. The increase of $\tau_{\rm rad}$ of anthracene derivatives by the binding of an Ar atom is small (10%–20%)[59] and cannot account for this effect. (ii) A small increase of the spin–orbit coupling by Ar, enhances k_{nr}. (iii) Vibrational predissociation within the (T_x) manifold of the complex, results in the broadening of the mediating states enhancing k_{nr}. For this mechanism to be operative, the energy gap between the $S_1(0)$ origin and of the electronic origin of the (T_x^k) manifold should exceed the binding energy ($D \simeq 700$ cm^{-1}) of the argon atom.[72] In any case, the dramatic disappearance of the inverse deuterium isotope effect in anthracene Ar_1 demonstrates the potential of vdW complexing in controlling the mediated interstate dynamics by the induction of the microscopic level shifts by vdW complexing.

E. Quantum yields from the electronic origins of some anthracene derivatives

Conventional wisdom has attributed the electronic relaxation from the S_1 manifold of anthracene and its derivatives to be dominated by ISC.[32–46] Qualitative correlations[60] indicate that the contribution of the $S_1 \rightarrow S_0$ internal conversion to electronic relaxation is minor, with the quantum yield for the populations of the S_0 channel being ~ 0.01. Accordingly, the absolute fluorescence quantum yields from the $S_1(0)$ electronic origins of five anthracene derivatives reported herein (Table IV) provide information on the general patterns of ISC in these compounds. The interstate nonradiative decay of $S_1(0)$ or any other vibronic state of S_1 may proceed by two interstate coupling mechanisms: (i) direct $|S_1\rangle - \{|T_1\rangle\}$ coupling which is characterized by the rate

$$\gamma_{\rm I}(S_1) = 2\pi |\langle S_1|V_{\rm so}|T_1\rangle|^2 \rho, \quad (4)$$

and (ii) mediated coupling whose rate is determined by the rate $\gamma_{\rm II}(S_1)$, Eq. (2). The total ISC decay rate $\gamma(S_1)$ of a S_1 state is given by the additive contribution

$$\gamma(S_1) = \gamma_{\rm I}(S_1) + \gamma_{\rm II}(S_1). \quad (5)$$

The unity quantum yield for the $S_1(0)$ electronic origins of 9,10-dichloroanthracene (9,10DCA) and of 9-cyanoanthracene (9CNA) imply that both decay channels (i) and (ii) are closed at this energy. Accordingly, direct $|S_1(0)\rangle - \{|T_1\rangle\}$ coupling is poor in these molecules, which are characterized by a medium spin–orbit coupling, while the electronic origin of the sparse mediating manifold is located above $S_1(0)$, or just slightly below it, so that no mediating vibrational state is in resonance with $S_1(0)$. The reduction of Y below unity for 9-methyl anthracene (9MA) is tentatively attributed to mechanism (ii) with $\gamma = \gamma_{\rm II}$, as is the case for anthracene and its deuterated derivatives, which were alluded to in Secs. III C and III D. Proceeding to the decay characteristics of $S_1(0)$ of molecules containing heavy atoms, which are characterized by a high spin–orbit coupling, i.e., bromoanthracene, we note the large three orders of magnitude difference between the quantum yields and the nonradiative decay rates of $S_1(0)$ of 9,10DBA for which $Y = 0.72$ and of 9BA for which $Y = 2.4\times10^{-3}$. The efficient ISC from $S_1(0)$ of 9BA ($Y = 2.4\times10^{-3}$) is attributed to the superposition of the direct mechanism (i) and the mediated mechanism (ii), both of which are enhanced by the internal heavy atom effect on the spin–orbit coupling terms $\langle S_1|V_{\rm so}|T_1\rangle$ in Eq. (4) and $\langle S_1|V_{\rm so}|T_x^k\rangle$ in Eq. (2). The operation of mechanism (ii) for 9BA implies that the electronic origin $T_x(0)$ of the mediating triplet is located below $S_1(0)$, ensuring effective resonance coupling between $S_1(0)$ and the mediating manifold. The dominating role of mechanism (ii) in 9BA is reflected by the dramatic differences between the Y values from $S_1(0)$ of 9BA ($Y = 2.4\times10^{-3}$) and of 9,10DBA ($Y = 0.72$). The modest heavy atom effect on ISC from $S_1(0)$ of 9,10DBA is due solely to the enhancement of the direct mechanism (i) by the internal spin–orbit effect, while the mediating channel (ii) is blocked, with $T_x(0)$ being located above $S_1(0)$ in this molecule. Thus, in 9,10DBA $\gamma = \gamma_{\rm I}$, while in 9BA $\gamma \simeq \gamma_{\rm I} + \gamma_{\rm II}$ with $\gamma_{\rm II} \gg \gamma_{\rm I}$, due to the dominating contribution of near-resonant mediating states to ISC.

Up to this point we were concerned with the ISC from the electronic origins. Under the circumstances, the exclusive nonradiative decay channel involves interstate electronic relaxation. We now proceed to explore the decay characteristics of higher vibrational excitations in the S_1 manifold, which may involve the combination of interstate

TABLE III. Quantum yields for the $S_1(0)$ origin of Ar complexes.

Molecule	Y	$k_{nr}\tau_{\rm rad}$
Anthracene-H_{10}	0.67	0.49
Anthracene-H_{10} Ar	0.49	1.04
Anthracene-D_{10}	0.134	6.69
Anthracene-D_{10} Ar	0.50	1.00

TABLE IV. Quantum yields from the $S_1(0)$ electronic origin of anthracene derivatives.

Molecule	(cm^{-1})[a]	Y[b]	$k_{nr}\tau_{\rm rad}$
9-methylanthracene	26 943	0.58	0.75
9-cyanoanthracene	26 171	1.00	···
9,10-dichloroanthracene	25 950	1.00	···
9,10-dibromoanthracene	25 877	0.72	0.39
9-bromoanthracene	26 724	0.0024	416

[a] Accuracy of peak position ± 3 cm^{-1}.
[b] Accuracy of absolute quantum yields is estimated to be 3%.

electronic relaxation and intrastate vibrational energy redistribution (IVR).

F. Vibrational level structure of anthracene and its derivatives

The vibrational excitations of anthracene in the S_1 manifold, which were obtained by LMIF and absorption spectroscopy (Fig. 11) and the vibrational level structure of anthracene in the S_0 state, which was obtained from dispersed fluorescence resulting from excitation into $S_1(0)$ (Fig. 12), are in excellent agreement with the LIF (laser-induced fluorescence) data of Zewail *et al.*[18] and with model calculations.[61] The vibrational level structure of the S_1 state for perdeutroanthracene MeA, 9CNA, 9,10DCA, 9,10DBA, and 9BA is displayed in a concise way in Figs. 16–21, and is confronted in Table V with the characteristic vibrations of anthracene. Seven prominent a_g vibrations out of 15 were easily identified in the S_1 state of anthracene-H_{10} which exhibit only a small energetic shift between S_0 and S_1 (Table V). The 387, 1168, 1380, 1420, and 1514 cm^{-1} (or 1554 cm^{-1}) vibrations in the S_1 manifold of anthracene-H_{10} exhibit a weak dependence on chemical substitution in the ninth or the ninth and tenth positions (Table V). The ~750 cm^{-1} a_g vibration in anthracene-H_{10} is expected to be drastically shifted by isotopic and chemical substitution,[61] so that the prominent vibrational feature in the range of 700–800 cm^{-1} for substituted anthracenes corresponds to a progression or combination band(s). The unique assignment of the S_1 vibrational structure above 700 cm^{-1} is complicated by the appearance of Fermi resonances (Table V), which essentially originate from intrastate anharmonic coupling effects and result in splittings of 1–10 cm^{-1}.[8] Typical examples are the 748, 755, and 766 cm^{-1} bunch of states and the 1380, 1409, and 1420 cm^{-1} bunch of states in the S_1 level structure

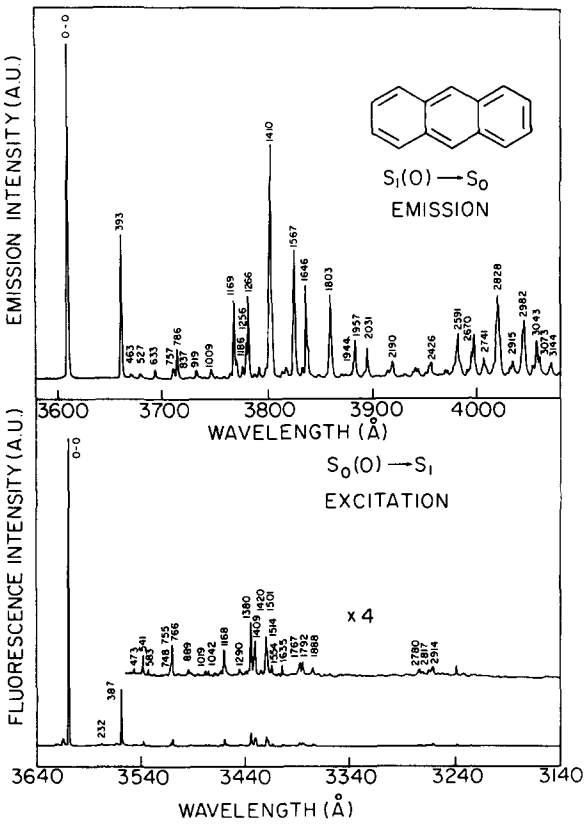

FIG. 12. Fluorescence excitation spectrum of anthracene at spectral resolution of 2 cm^{-1} (lower curve) and energy resolved emission from $S_1(0)$ of anthracene at spectral resolution of 5 cm^{-1} (upper curve). Numbers represent the vibrational excitations above the electronic origins of S_1 or of S_0.

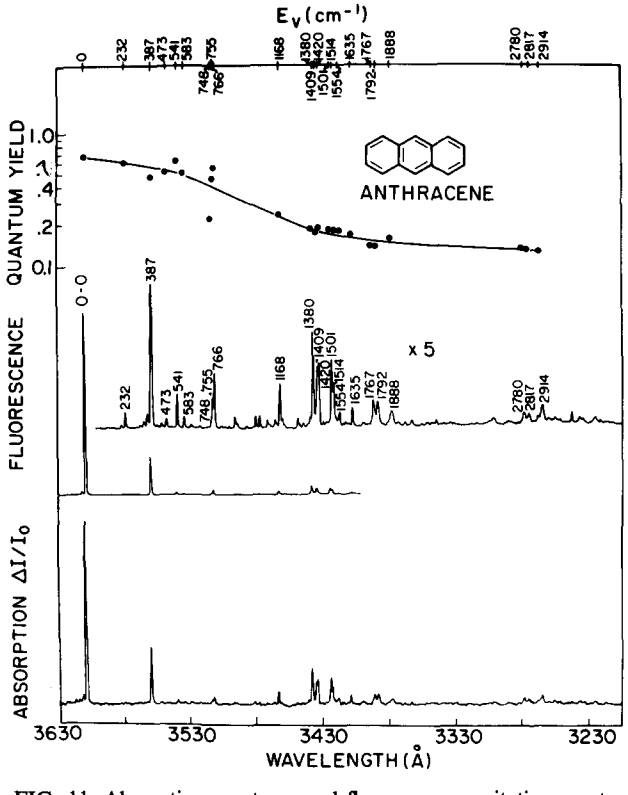

FIG. 11. Absorption spectrum and fluorescence excitation spectrum of anthracene-H_{10} over the range 3630–3230 Å. $P = 130$ Torr, $T = 138$ °C, and $X = 6$ mm, spectral resolution 3 cm^{-1}. The numbers represent the vibrational excitations above the S_1 electronic origin in cm^{-1}. The points (● ● ●) represent the absolute fluorescence quantum yields. The upper curve was drawn for the sake of visual display.

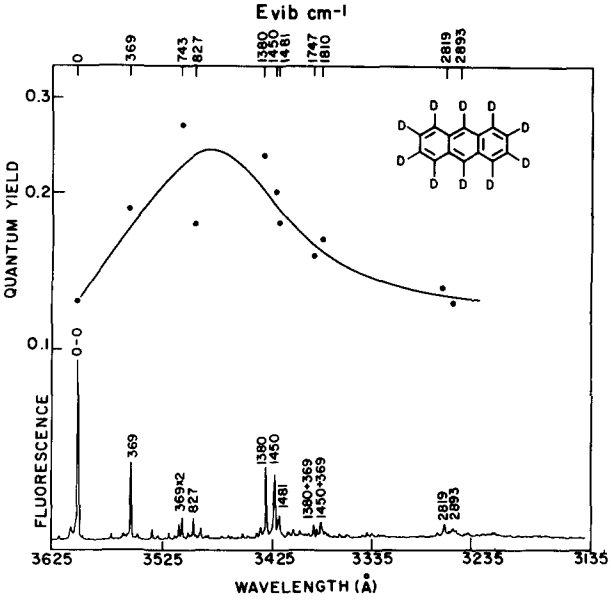

FIG. 13. Fluorescence excitation spectrum and absolute fluorescence quantum yields of anthracene-D_{10} in the spectral range 3625–3235 Å. $P = 110$ Torr, $T = 130$ °C, and $X = 6$ mm. Notation as in Fig. 11.

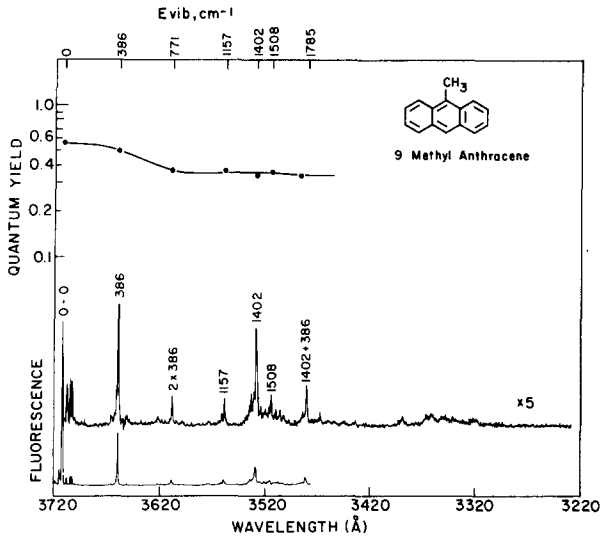

FIG. 14. Fluorescence excitation spectrum and absolute fluorescence quantum yields of 9-methyl anthracene in the spectral range 3720–3220 Å. $P = 110$ Torr, $T = 130$ °C, and $X = 6$ mm. Notation as in Fig. 11.

of anthracene (Fig. 19). These Fermi resonances provide one type of intrastate anharmonic interactions[65–67] which, together with the Coriolis interaction[54–56] are responsible for IVR at higher energies, where the S_1 manifold becomes denser.

Another interesting implication of Fermi resonance effects is the breakdown of the mirror symmetry between the absorption (or LMIF) spectrum and the energy-resolved emission spectra at higher excess vibrational energies. A cursory examination of Figs. 12 and 20 reveals that the

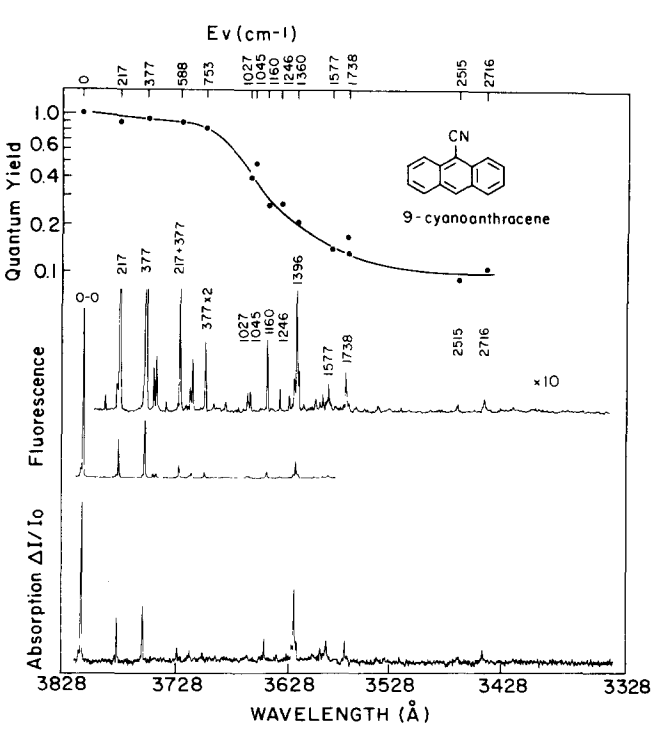

FIG. 15. Absorption spectrum fluorescence excitation spectrum and absolute fluorescence quantum yields of 9-cyanoanthracene in the spectral range 3828–3328 Å. $P = 110$ Torr, $T = 135$ °C, and $X = 6$ mm. Notation as in Fig. 11.

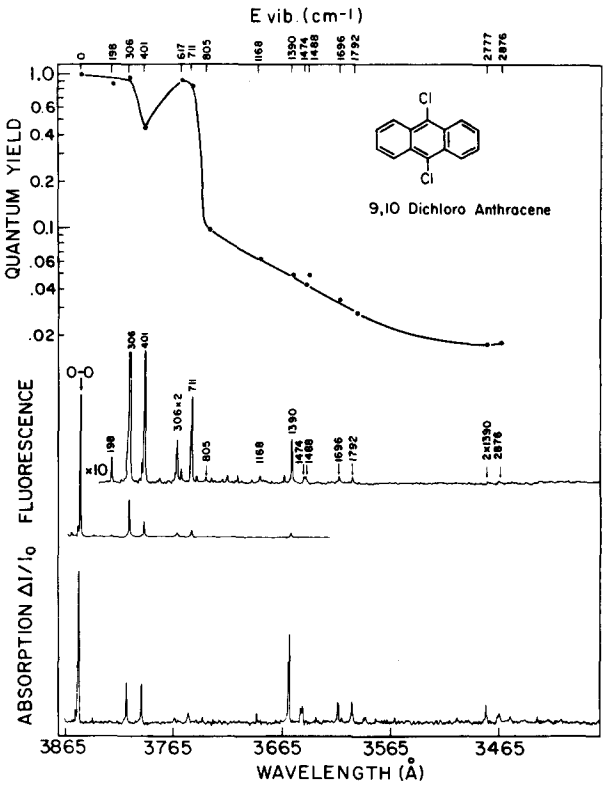

FIG. 16. Absorption spectrum, fluorescence excitation spectrum, and absolute fluorescence quantum yields of 9,10-dicloroanthracene over the spectral range 3865–3375 Å. $P = 100$ Torr, $T = 140$ °C, and $X = 6$ mm. Notation as in Fig. 11.

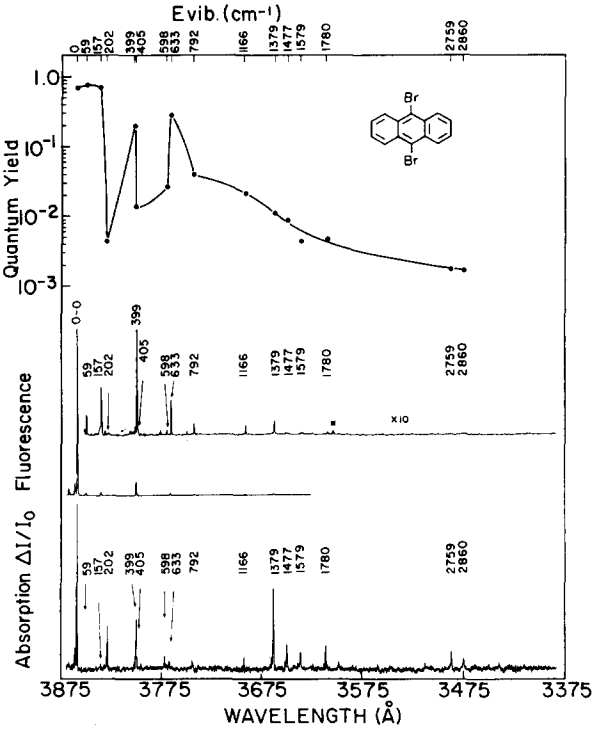

FIG. 17. Absorption spectrum, fluorescence excitation spectrum, and absolute fluorescence quantum yields 9, 10-dibromoanthracene over the spectral range 3875–3375 Å. $P = 100$ Torr. $T = 145$ °C, and $X = 6$ mm. Notation as in Fig. 11.

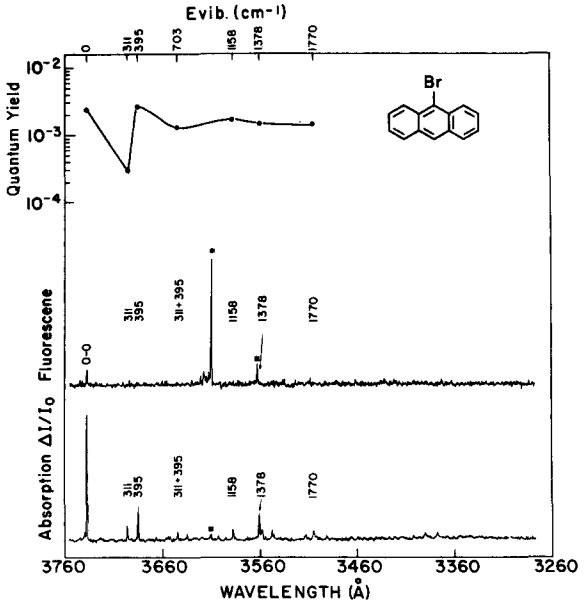

FIG. 18. Absorption spectrum, fluorescence excitation spectrum, and absolute fluorescence quantum yields of 9-bromoanthracene over the spectral region 3760–3260 Å. $P = 100$ Torr, $T = 145$ °C, and $X = 6$ mm. Notation as in Fig. 11. The spectral features in the LMIF spectrum marked by a star (*) correspond to an impurity of anthracene.

$S_0(0) \rightarrow S_1$ absorption (or fluorescence excitation) and the fluorescence from $S_1(0)$ spectra exhibit a mirror image for $E_v \simeq 0$–800 cm^{-1}, while for $E_v > 800$ cm^{-1} this mirror symmetry is broken. As is evident from Fig. 12, the 1410 cm^{-1} vibrational excitation in S_0 is replaced by the Fermi resonance mates 1380, 1409, and 1420 cm^{-1} in S_1 of anthracene. Interesting effects of the breakdown of mirror symmetry are exhibited for 9,10DCA (Fig. 20), where the S_1 manifold reveals the prominent 1390 cm^{-1} vibration, which is replaced by the pair 1406 and 1273 cm^{-1} in S_0. The appearance of the 1273 cm^{-1} feature in S_0 may originate from intensity sharing due to Fermi resonance effects, between the 1406 and 1273 cm^{-1} excitations, while the counterpart of the latter excitation is absent in S_1. Alternatively, the 1273 cm^{-1} in S_0 of 9,10DCA may originate from a vibration which suffers a large frequency change between the two electronic states. Another manifestation of the breakdown of the mirror symmetry pertains to the intensity alternation between the absorption and the emission spectra. As is evident from Fig. 12, the relative peak intensity of the 1410 cm^{-1} vibrational excitation in S_0 is considerably higher than the sum of the relative intensities, which are corrected for the quantum yield, of the 1380, 1409 cm^{-1} manifold in S_1. Similarly, in the spectrum of 9,10DCA (Fig. 20), the 1390 cm^{-1} vibration in S_1 is more intense than the corresponding 1406 cm^{-1} in S_0. A mirror symmetry breakdown between absorption and fluorescence can be attributed to the following effects: (1) interference between vibronically induced and allowed transition moments,[68,69] (ii) normal coordinate rotation in S_1,[70,71] and (iii) Fermi resonance anharmonic mixing. Effect (i) is expected to be significant only for symmetric levles of a moderately weak electronic transition, being of minor importance for the strongly allowed $S_0 \rightarrow S_1$ transition of anthracene and its derivatives. Nothing is presently known regarding the Duschinsky rotation[70] [effect (ii)] in the S_1 manifold, which may modify the vibronic intensities of the $S_1(0) \rightarrow S_1$ transition but not the $S_1(0) \rightarrow S_0$ emission spectrum.[71] The splitting of the higher levels in S_1, e.g., the appearance of the 1380, 1409, and 1420 cm^{-1} manifold in the S_1 state of anthracene (Fig. 12) points towards the significant role of Fermi resonance effects in the mirror symmetry breakdown.

Of some interest are the low frequency S_1 vibrations of substituted anthracene, which involve the motion of the substituents. The very low frequencies (31 and 54 cm^{-1}) exhibited for 9MeA correspond to the hindered rotation of the CH_3 group.[62] The 306 cm^{-1} vibration of 9,10DCA involves the motion of the Cl atoms in view of the marked Cl isotope effect on this frequency,[63] while the 202 cm^{-1} vibration of 9,10DBA may correspond to the analogous vibration involving the Br atoms. Another mode in this category involves the 311 cm^{-1} vibration of 9BA, which corresponds to the motion of the Br atom in this compound.

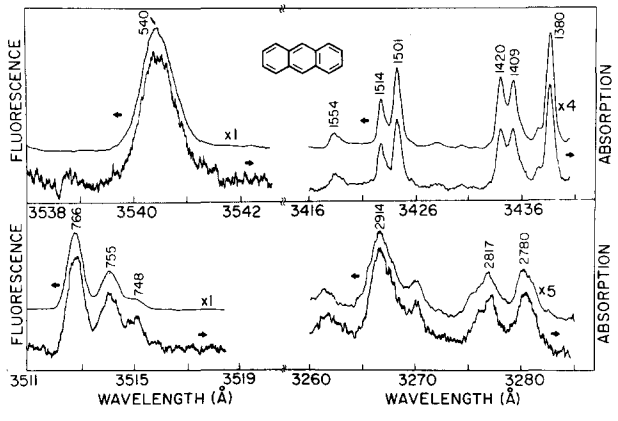

FIG. 19. Some details of the absorption and fluorescence excitation spectra of anthracene. Experimental conditions and notation as in Fig. 11.

G. Nonradiative decay rates of anthracene and excess vibrational energy dependence of pure radiative lifetimes

The dependence of the fluorescence quantum yields from photoselected vibrational excitations in the S_1 manifold of anthracene is portrayed in Fig. 11. Our quantum yield data were combined with the lifetime τ data of Zewail *et al.*[19] to provide the dependence of the nonradiative decay rates $k_{nr} = (1 - Y)/\tau$ and the pure radiative lifetimes $\tau_{rad} = \tau/Y$ over the excess vibrational energy range $E_v = 0$–3300 cm^{-1} above the $S_1(0)$ origin (Fig. 21). The pure radiative lifetime of the $S_1(a_g)$ states in the low-energy domain ($E_v = 0$–800 cm^{-1}) are practically independent of E_v, falling in the range $\tau_{rad} = 33$–38 ns as expected for a symmetry-allowed transition. Notable exceptions from this rule involve the weak 232 ($\tau_{rad} = 47$ ns),the 540 ($\tau_{rad} = 57$ ns), and the 748 cm^{-1} ($\tau_{rad} = 50$ ns) vibrational features, whose pure radiative lifetimes exceed by about 50% the τ_{rad} values for the electronic origin and the low-lying $S_1(a_g)$ states (Fig. 22). These weak "abnormal" spectral features were tentatively

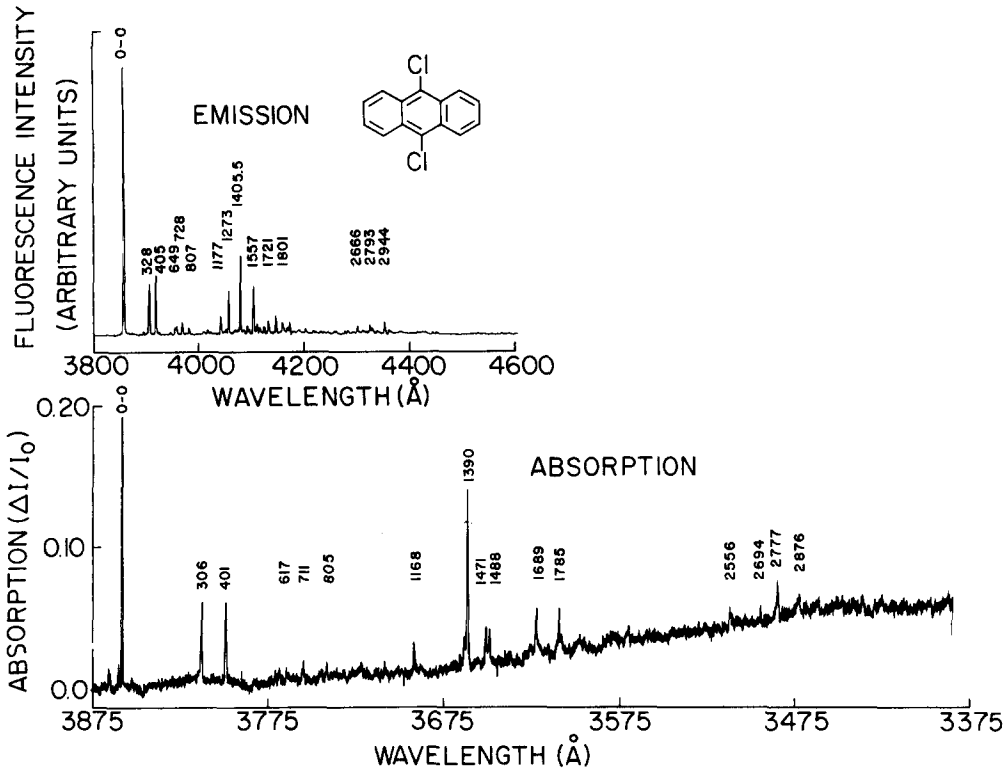

FIG. 20. Absorption spectrum at spectral resolution of 4 cm^{-1} (lower trace) and energy resolved emission from $S_1(0)$ at spectral resolution of 7 cm^{-1} (upper trace) of 9,10-dichloroanthracene. The baseline shift of the absorption spectrum is not genuine and is corrected electronically (see Sec. II) in Fig. 16.

attributed to vibronically induced transitions. Nonresonant vibronic coupling effects originating from Duschinsky rotation of the excited-state normal coordinates may result in the reduction of the transition moment for emission from a nontotally symmetric vibronic state,[70,71] resulting in the lengthening of τ_{rad}. In the higher energy domain ($E_v = 1100$–2800 cm^{-1}) the τ_{rad} values are slightly higher than the radiative lifetimes for the $S_1(a_g)$ states in the low energy region, spanning the range 38–45 ns. Vibronic coupling effects may be operative for the "background" S_1 states in the high energy domain, which becomes populated by IVR[54–56] and which becomes active in $S_1 \rightarrow S_0$ emisison, resulting in the increase of τ_{rad} and are of interest. However, the overall nearly constant values of τ_{rad} over a broad E_v range (Fig. 22) imply that the $k_{nr}\tau_{rad}$ data inferred from our experimental Y values can be used to extract estimates of the vibrational energy dependence of k_{nr}, which are reliable within 15%, or so. The quantum yield data for the variety of anthracene derivatives (Figs. 16–21) provide a wealth of semiquantitative information on intramolecular dynamics.

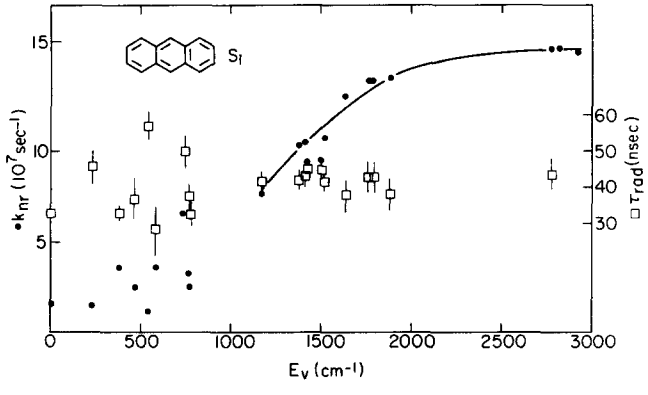

FIG. 21. The dependence of the nonradiative decay rates k_{nr} and of the pure radiative lifetimes τ_{rad} of anthracene on the excess vibrational energy above the $S_1(0)$ electronic origin.

H. General trends of the excess vibrational energy dependence of k_{nr}

The excess vibrational energy dependence of the nonradiative rates from the S_1 manifold of anthracene (Fig. 21) exhibit three energy domains:

(A) The low energy region $E_v < 800$ cm^{-1} where irregular variation of k_{nr} values is revealed, exhibiting mode specificity of the electronic relaxation rates.

(B) The intermediate energy region $800 < E < 1800$ cm^{-1}, where k_{nr} increases practically monotonically with increasing E_v.

(C) The high energy domain $E_v > 1800$ cm^{-1} where k_{nr} exhibits a weak dependence on the excess vibrational energy.

An examination of the E_v dependence of the quantum yields for anthracene (Figs. 11 and 21) perdeuteroanthracene (Fig. 13), 9MeA (Fig. 14), and 9CNA (Fig. 15) reveals similar characteristics. In particular, it should be noted that regions (B) and (C) seem to be exhibited in all these molecules. These universal characteristics of the interstate electronic relaxation in regions (B) and (C) of large mole-

TABLE V. Vibrational level structure of anthracene and some of its derivatives.[a]

Anthracene-H_{10}	Anthracene-D_{10}[c]	9MeA	9CNA	9,10DCA	9,10DBA	9BA
232(S_0)		31,54,68[d]	217[e]	198	59	
				306[f]	157	
					202[g]	311
387(S_1), 393(S_0)	369	386	377	401	399	395
[369 (a_g)]	[361 (a_g)]				405	
					[2×202]	
473(S_1), 463(S_0)						
541(S_1), 527(S_0)						
[517 (b_{3g})]						
583(S_1), 633(S_0)					598	
					[202 + 399]	
					633	
748(S_1), 755(S_1),						
766(S_1)						
757(S_0), 783(S_0)	743	711	753	710	792	703
[735(A_g)] + 2×387						
+ FRS[h]	[2×369]	[2×386]	[2×377]	[2×306][a]	[2×395]	[33 + 395]
1168(S_1), 1169(S_0)	827	1157	1160	1168	1166	1158
[1169(a_g)]	846(a_g)					
1266(S_0)			1246			
[1240(a_g)]						
1380(S_1), 1410(S_0)	1380	1402	1396	1390	1379	1378
[1398(a_g)] + FRS	[1347(a_g)]					
1409(S_1), 1420(S_1)	1450			1474	1477	
1514(S_1), 1567(S_0)	1481	1508		1488		
[1557(a_g)]						
1554(S_1)			1577		1579	

[a]All energies are given relative to the electronic origin of the molecule (in cm^{-1}).

[b]For anthracene-H_{10} we present the energies of the S_1 manifold [marked (S_1)] and of the S_0 manifold [marked (S_0)]. For all other compounds the energies of the S_1 manifold is presented.

[c]Calculated a_g (allowed) and b_{3g} (vibronically induced) vibrational frequencies for the S_0 manifold, which were taken from the work of Califano *et al.* [Ref. 61(a)] and of Ohno [Ref. 61(b)], are marked [(a_g)] and [(b_{3g})]. FRS denotes Fermi resonances.

[d]The low frequencies for the hindered rotation of the Me group.

[e]Low frequency motion of the CN group.

[f]Motion of Cl groups.

[g]Motion of Br group(s).

[h]For vibrational energies exceeding 700 cm^{-1}, Fermi resonance effects make vibrational assignment uncertain.

cules is related to the effects of intrastate intramolecular vibrational energy redistribution (IVR).

The manifestations of intrastate IVR can be inferred from the appearance of Fermi resonances in the $S_0 \rightarrow S_1$ absorption (or LIF) spectra,[9,18] the splitting and broadening of the energy-resolved $S_1 \rightarrow S_0$ emission[18] and the exhibition of quantum beats in the simultaneous time-resolved and energy-resolved decay.[66–68] The study of Felker and Zewail on IVR in the S_1 manifold of anthracene[66–68] indicates that region (B) corresponds to the intermediate level structure for intrastate mixing, while region (C) corresponds to the statistical limit for IVR. Regarding the manifestations of IVR on electronic relaxation it has already been proposed[8,64] that the features of range (C) originate from efficient IVR in the S_1 manifold, i.e., the statistical limit for IVR which affects the dynamics of the mediated $S_1 \rightarrow T$ crossing. We assert that range (B) corresponds to the intermediate level structure of IVR within the S_1 manifold, which results from anharmonic or/and Coriolis interactions. It has been suggested[66–69] that the anharmonic interactions provide a dominating contribution to the intrastate coupling. Recent studies on rotational state dependence of the time-resolved decay and of fluorescence quantum yield from vibronic states in range (B) of 9CNA demonstrate the significant role of Coriolis interactions.[55,56,64] From these considerations the following picture emerges of intramolecular dynamics in the S_1 manifold of these substituted anthracenes. Range (A) corresponds to the sparse level structure in S_1, where intrastate coupling does not prevail and each individual S_1 level may undergo (direct or mediated) ISC to T_1. In range (B) intrastate interaction couple a S_1 doorway state, which carries oscillator strength from the ground state origin $S_0(0)$ with background S_1 states, which do not carry oscillator strength from $S_0(0)$. The scrambled S_1 manifold exhibits a mediated ISC to the statistical T manifold. The major cause for the decrease of Y with increasing E_v in range (B) is attributed to the difference in the nonradiative decay rates of the doorway state(s) and of the background states. On the basis of the experimental data, we assert that the nonradiative ISC rates of the background S_1 states exceed that of the S_1 doorway states. This is reasonable, as different symmetries of these levels will affect the Franck–Condon factors which determine ISC. Range (C) corresponds to the statistical limit of IVR, where the S_1 doorway states decay nonradiatively to

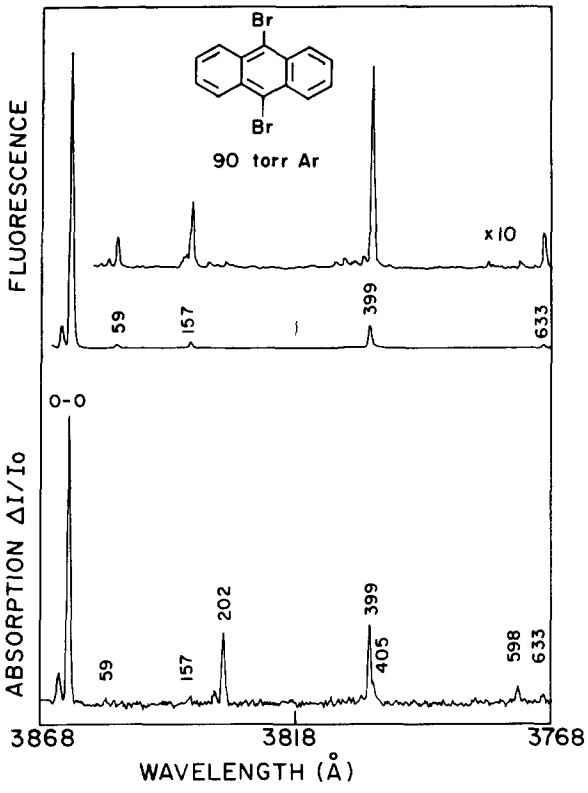

FIG. 22. Details of the absorption (lower trace) and fluorescence excitation (upper trace) spectra of 9,10-dibromoanthracene in the range 3868–3768 Å. Note the huge drop between the fluorescence quantum yield at 202 cm^{-1} relative to 0–0 and 157 cm^{-1}.

dense manifold of background S_1 states, which in turn decay to the T manifold. The interstate dynamics, which is manifested by the fluorescence quantum yield, is then governed by the decay rates of the S_1 background states.

The existence of domains (B) and (C) seems to be universal[64] and was observed in the S_1 manifold of many other large molecules, e.g., tetracene,[8] pentacene,[10] perylene,[31] fluorene,[31] and carbazole.[31] This universality inspires confidence in the admittedly qualitative picture, which rests on the coupling between intrastate IVR and interstate electronic relaxation. Regarding the interstate coupling we have already noted that the dynamics of electronic origins cannot be described in terms of the simple-minded picture for direct $S_1 - (T_1)$ coupling, and mediated coupling has to be invoked. These mediating coupling effects are manifested in the E_v dependence of Y of 9,10DCA and 9,10DBA, which will now be considered.

I. Resonance effects in the E_v dependence of ISC dynamics

We have seen in Sec. III E that for the electronic origins of 9,10DCA the ISC is blocked while the electronic origin of 9,10DBA is practically immune with respect to ISC, exhibiting modest electronic relaxation due to direct ISC. As these molecules are characterized by medium (for 9,10DCA) and high (for 9,10DBA) intramolecular spin–orbit coupling, we expect that the onset of mediated ISC will be manifested by a large abrupt drop of Y with increasing E_v. This expectation is borne out by the E_v dependence of Y for 9,10DCA, where the fluorescence quantum yield reveals a dip at 401 cm^{-1} and drops by a numerical factor of 9 in the energy domain between 617 and 805 cm^{-1} and retains a low value at higher E_v (Fig. 16). This pattern is attributed to the onset of mediated ISC at $E_v \geqslant 401$ cm^{-1} with the 401 cm^{-1} state being already coupled to the $\{|T_x^k\}$ manifold, while efficient coupling with the mediating $\{T_x^k\}$ manifold sets in at the energy domain 711–805 cm^{-1}. A more interesting and detailed manifestation of the onset of mediated coupling at finite E_v is exhibited in 9,10DBA. In Figs. 22 and 23 we present the low-energy LMIF and absorption spectra of 9,10DBA, which exhibit clearly the high value of Y at the origin and at the 157 and 399 cm^{-1} vibration with the huge decrease of Y at 202 (Fig. 22) and at 405 cm^{-1} (Fig. 23) vibrations. It is extremely interesting to note that a small shift of the S_1 vibrational energy by 6 cm^{-1} from 399 to 405 cm^{-1} results in a twentyfold decrease in Y, while a shift of 35 cm^{-1} from 598 to 633 cm^{-1} leads to a thirtyfold increase of Y. It is also interesting to note that the three vibrational excitations of 202, 405 (2×202), and 598 cm^{-1} (202 + 399), which exhibit low Y value for 9,10DBA, involve the Br atom vibrations, pointing towards mode specificity in the $S_1 - \{T_x^k\}$ coupling. The three marked minima in the oscillatory energy dependence of Y vs E_v can be accounted for in terms of near resonances between the following pairs of levels: (i) $T_x(0)$ with S_1 (202 cm^{-1}), (ii) $T_x(0) + 202$ cm^{-1} with S_1 (405 cm^{-1}), and (iii) $T_x(0) + 399$ cm^{-1} with S_1 (598 cm^{-1}). The near-resonant interaction between the portions of the S_1 and $\{T_x\}$ manifolds will considerably enhance the interstate coupling of these specific S_1 levels, while other states in the

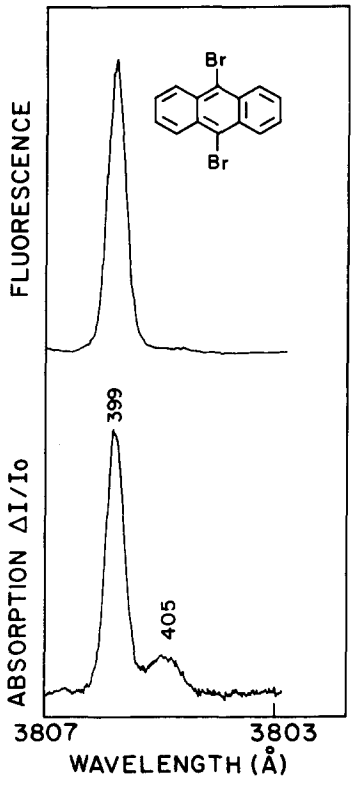

FIG. 23. Details of the absorption and fluorescence excitation spectra of 9,10-dibromoanthracene in the range 3807–3803 Å. Note the dramatic difference in the fluorescence quantum yield between 399 and 405 cm^{-1}.

S_1 manifold in this energy domain are not effectively coupled to the mediating states. The remarkable oscillatory energy dependence of Y together with the energetic sensitivity of the ISC rates (Fig. 17) is attributed to accidental near degeneracies between the S_1 doorway state(s) in the range 202–800 cm^{-1} and the mediating states in the $\{T_x^k\}$ manifold. According to our picture the details of the $S_1 - \{T_x\}$ energetics will determine the quantitative details of the ISC rates. The physical picture based on resonance effects is extremely attractive. Further experimental confirmation of the role of $S_1 - \{T_x\}$ resonance effects was obtained from the study of the implications of level shifts of the 202 cm^{-1} vibration induced by complexing and by isotopic analysis of 9,10DBA.

We have studied the fluorescence quantum yields of 9,10DBA Ar complexes at low vibrational excitations. In Fig. 24 we present the absorption and the LMIF spectra of 9,10DBA expanded in Ar at several stagnation pressures p of the diluent. Several hot bands of 9,10DBA are suppressed with increasing p, e.g., the 146 cm^{-1} features (Fig. 24). In addition to the bare molecules 157 and 202 cm^{-1} vibrations a new feature appears at 151 cm^{-1}. The relative intensity of this 151 cm^{-1} new feature strongly increases with increasing stagnation pressure. Accordingly, the 151 cm^{-1} feature is attributed to a vibrational excitation of the 9,10DBA Ar_1 complex. The spectral shift of the electronic origin of 9,10DBA Ar_1 relative to $S_1(0)$ of 9,10DBA was found to be -50 ± 2 cm^{-1}. A similar shift is expected for intramolecular vibrational excitations of 9,10DBA Ar_1. Thus the 151 cm^{-1} excitation is assigned to the 202 cm^{-1} intramolecular vibrational excitation of the 9,10DBA Ar_1 complex. The red spectral shift is attributed to dispersive stabilization[72] of S_1 (202 cm^{-1}) relative to $S_0(0)$. On the other hand, the stabilization of the mediating (T_x^k) manifold by dispersive interactions is smaller than that of S_1. We thus expect that the energy defect(s) $|E(S_1(202) - E(T_x)|$ which determine the mediated ISC rate according to Eq. (2), will be grossly modified by Ar complexing. While in the bare molecule near-resonant interaction between S_1 (202 cm^{-1}) and some (T_x) levels prevails, the dispersive level shift of S_1 (202 cm^{-1}) will destroy the near accidental degeneracy resulting in a dramatic enhancement of Y from the S_1 (202 cm^{-1}) level of the Ar complex relative to that of the bare molecules. In Table VI we present the quantum yield data for the low vibrational levels of 9,10DBA Ar. The two orders of magnitude increase of Y for the 202 cm^{-1} vibration in the complex is attributed to the energetic "liberation" of this level from near-resonant coupling, which is induced by complexing. Alternative interpretations of the dramatic enhancement of Y for this vibrational excitation should be considered. One possibility involves vibrational predissociation of the 9,10DBA Ar complex. However, from extensive model calculations and experimental data[72] for the dissociation energies of large vdW complexes it is apparent that the dissociation energy of the 9,10DBA Ar complex should be 500–600 cm^{-1} (Ref. 72) so that the reactive vibrational predissociation channel is closed at 202 cm^{-1}. Another mechanism for the intramolecular dissipation of the intramolecular vibrational energy may involve nonreactive IVR between the intramolecular 202 cm^{-1} vibration and the low-frequency molecule-Ar vibration within the complex. This process, which cannot be excluded at present, will eliminate the near-resonant $|E(S_1(202) - E(T_x)|$ coupling due to dynamic effects.

Level shifts of the S_1 (202 cm^{-1}) vibrational excitation relative to the $\{T_x\}$ manifold in 9,10DBA can be induced by isotopic substitution of the Br atom. In Fig. 25 we portray an interesting energy dependence of the quantum yield within the contour of the 202 cm^{-1} excitation, which reveals a drop

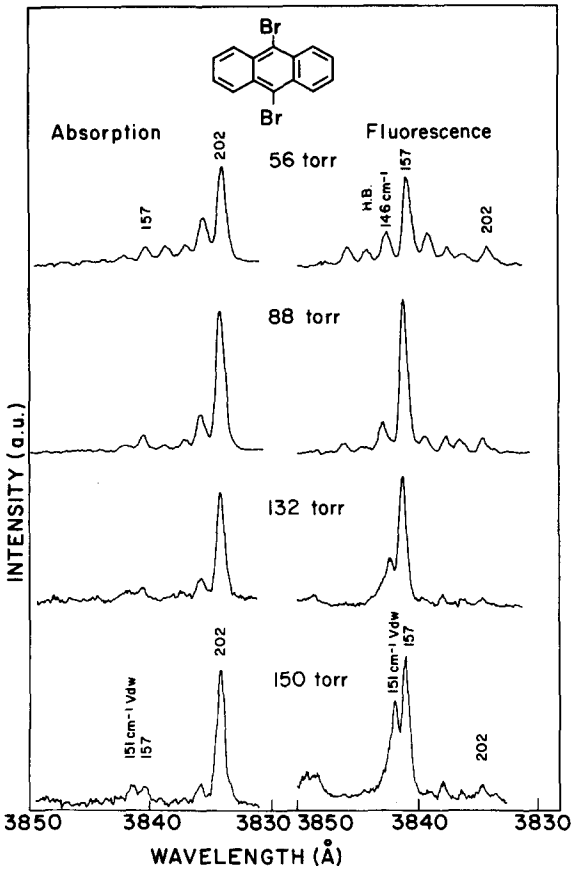

FIG. 24. Absorption spectra (left-hand side curves) and fluorescence excitation spectra (right-hand side curves) of 9,10 dibromoanthracene at several stagnation pressures of Ar, which are marked on the spectra. All the spectra reveal the 157 cm^{-1} and the 202 cm^{-1} features, which correspond to S_1 vibrational excitation of the bare molecules. At low stagnation pressures $P = 56$ Torr and $P = 88$ Torr hot sequence bands of the bare molecules appear, the most prominent being the 146 cm^{-1} feature, which is marked *H.B.* The *H.B.* disappears at higher P. At $P = 132$ Torr and $P = 150$ Torr a new spectral feature appears at 151 cm^{-1} which is attributed to a 9,10DBA, Ar van der Waals complex.

TABLE VI. Fluorescence quantum yields from 9,10DBA and 9,10DBA Ar.

Energy[a] (cm^{-1})	9,10DBA	9,10DBA Ar
0	0.72	0.65
202	0.005	0.60

[a] Relative to electronic origin.

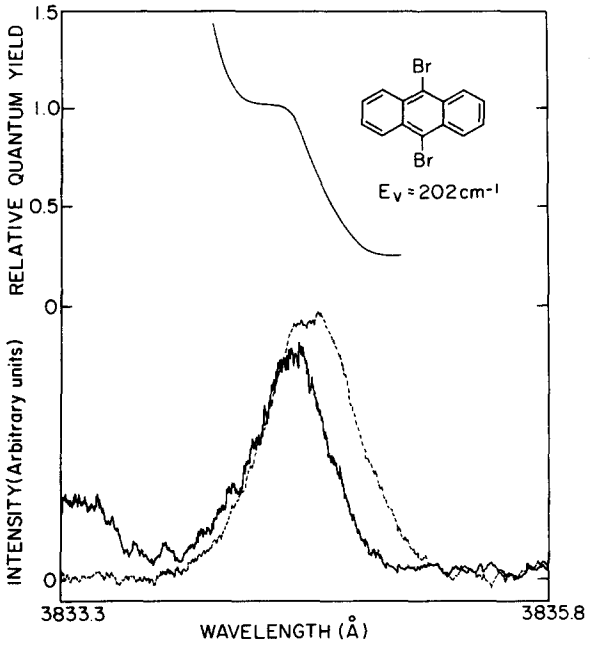

FIG. 25. Absorption spectrum (dashed lower curve), fluorescence excitation spectrum (solid lower curve), and relative fluorescence quantum yield (upper curve) across the (unresolved) contour of the 202 cm^{-1} S_1 excitation of 9,10-dibromoanthracene.

of Y at lower energies. The 202 cm^{-1} vibration of 9,10DBA, which involves the motion of the Br atoms, is expected to exhibit a marked Br isotope effect in an analogy to the 306 cm^{-1} vibration of 9,10DCA.[63] The 202 cm^{-1} contour of 9,10DBA consists of a superposition of the rotational contours of $Br^{79}Br^{79}$, $Br^{79}Br^{81}$, and $Br^{81}Br^{81}$ compounds with the relative shifts of 0.7 and 1.3 cm^{-1}. In contrast to the S_1 (202 cm^{-1}) excitation, the $\{T_x\}$ manifold does not necessarily involve Br atom vibrational motion and is not markedly affected by isotopic substitution. Accordingly, the $|E(S_1(202)) - E(T_x)|$ energy defects are modified by the Br isotopic substitution, with small energy shifts resulting in a dramatic one order of magnitude change of the mediated ISC rate.

We have attributed the remarkable oscillatory dependence of Y vs E_v in 9,10DBA to near-resonant effects between some vibrational excitation of S_1 and the $\{T_x\}$ manifold. This mechanism is consistent with the manifestation of the energetic level shifts of S_1 induced by intermolecular complexing or by intramolecular isotopic substitution. A marked oscillatory dependence of Y vs E_v is also exhibited in the low E_v domain of 9BA (Fig. 18), where at $E_v = 311$ cm^{-1} Y drops by about one order of magnitude. The extremely low Y values for 9BA imply that the mediating mechanism is operative already for $S_1(0)$ and for all vibrational excitations of S_1. Accordingly, the drop of Y for S_1 (311 cm^{-1}) for 9DBA cannot be attributed to near-resonant effects with the $\{T_x\}$ manifold. The 311 cm^{-1} of 9BA involves the motion of the Br atom and the surprising reduction of Y for this state may originate from mode specificity in the $S_1 - \{T_x\}$ coupling. An attractive possibility exists that the resonances in Y observed both in 9,10DBA and 9BA are partially due to an enhanced coupling strength of those vibrational states involving bromine atoms motion with the mediating $\{T_x^k\}$ manifold. The nature of mode specificity in mediated ISC deserves a further study.

J. Coupling between IVR and mediated ISC

The intramolecular dynamics in the S_1 manifold of anthracene and its derivatives is dominated by the interplay between two classes of intramolecular interaction:

(i) Intrastate coupling involving anharmonic and/or Coriolis coupling which does not prevail for $S_1(0)$ but sets in with increasing E_v.

(ii) Interstate coupling involves two types: (a) very weak direct spin–orbit coupling which prevails only when the intramolecular spin–orbit interaction is appreciable, i.e., 9,10DBA; (b) mediated spin–orbit and vibronic coupling Eq. (1), which dominates the ISC. The dominant role of mediated coupling in this class of compounds emerging from our data is evident from the inverse deuterium isotope effect on ISC at the origin, the sensitivity of k_{nr} of $S_1(0)$ to isotopic substitution, the erosion of the inverse isotope effect by Ar complexing, the stepwise onset of ISC in 9,10DCA, the resonance effects on ISC in 9,10DBA and their modification by Ar complexing.

The intrastate coupling depends on the excess vibrational energy, while the nature of the mediated interstate coupling depends on the nature of the molecule. In Fig. 26 we present the relevant coupling schemes which are encountered in this class of compounds. The following cases were documented:

(1) The interstate $S_1 - \{T_1\}$ coupling to the statistical limit, while intrastate coupling does not prevail. This situation corresponds to the $S_1(0)$ origins of 9CNA, 9,10DCA, and 9,10DBA. ISC is very inefficient, being exhibited only for $S_1(0)$ of 9,10DBA.

(2) The interstate coupling S_1–$\{T_x^k\}$–$\{T_1\}$ is mediated with the sparse $\{T_x\}$ manifold while $T_x^k \rightarrow \{T_1\}$ coupling is statistical. No intrastate coupling prevails. This situation corresponds to (i). The $S_1(0)$ origin and low vibrational excitation, i.e., range (A) of anthracene, its deuterated anthracenes, and 9MA. (ii) The electronic origin and low vibrational excitation 9BA, where the very low quantum yield is due to the high spin–orbit interaction. (iii) Some vibrational excitations of 9,10DCA and 9,10DBA which exhibit resonance effects on ISC.

(3) The interstate coupling S_1–$\{T_x^k\}$–$\{T_1\}$ is mediated by the $\{T_1\}$ manifold, while intrastate coupling is effective in the S_1 manifold and corresponds to the intermediate level structure. This state of affairs corresponds to participation of both doorway and background S_1 states in the ISC process. This state of affairs corresponds to range (B) in anthracene, deuterated anthracenes 9CNA and 9BA.

(4) The interstate S_1–$\{T_x^k\}$–$\{T_1\}$ coupling is mediated, with the $\{T_x^k\}$ manifold being statistical. Intrastate coupling between the doorway and background S_1 states prevails and IVR corresponds to the statistical limit. The ISC rates are determined by the ISC rates of the background S_1 states, which decay to the statistical $\{T_x^k\}$ manifold. These ISC rates exhibit a weak E_v dependence. This state of affairs

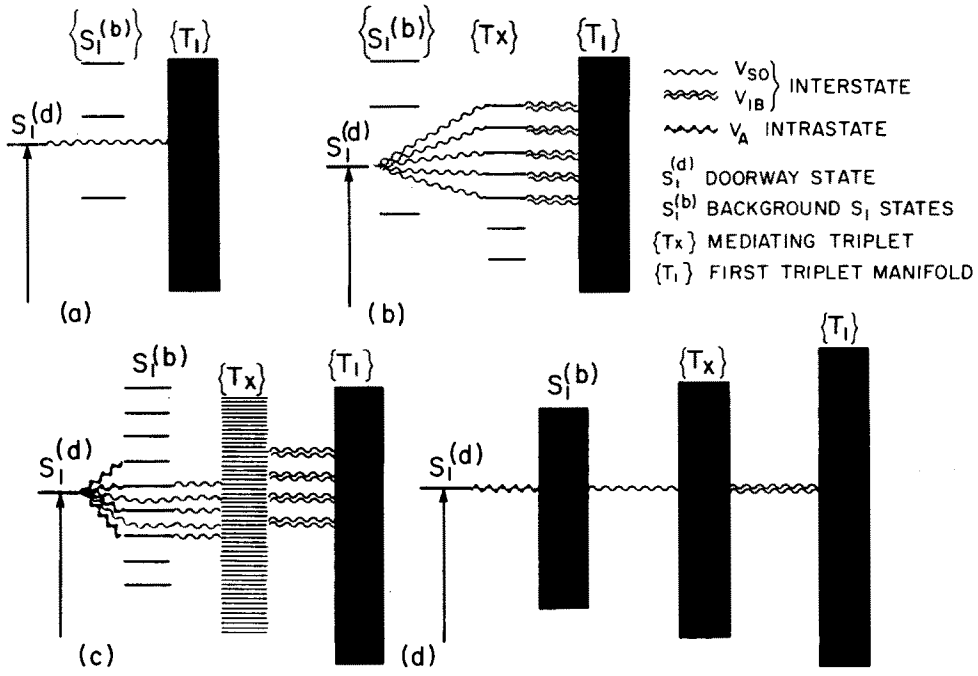

FIG. 26. Interstate and intrastate coupling schemes for intersystem crossing. (a) A doorway state of a very sparse S_1 manifold undergoing direct ISC to a (T_1) quasicontinuum. (b) A doorway state of a very sparse S_1 manifold undergoing mediated ISC through near-resonant coupling with a sparse (T_x) manifold. (c) The S_1 manifold becomes denser and intrastate coupling between the doorway state background S_1 states prevails. The mixed $S_1^{(d)} + S_1^{(b)}$ states decay via mediated ISC. (d) The $S_1^{(b)}$ and (T_x) manifolds are statistical relaxation and can be described in terms of sequential decay, i.e., $S_1^{(d)} \rightarrow (S_1^{(b)}) \rightarrow (T_x) \rightarrow (T_1)$, which corresponds to a sequence of IVR, ISC, and triplet–triplet internal conversion.

prevails at high values of E_v for all the anthracene derivatives in range (C). From the limiting high E_v quantum yields (Table VII) we infer that the ISC rates depend on the intramolecular spin–orbit coupling, as expected. In range (C) the ISC rates (Table VII) are weakly dependent on the position of the same classical substituents and on the isotopic substitution. The erosion of the inverse deuterium isotope effect in this range can be rationalized in terms of $\{S_1\} \rightarrow \{T_x^k\}$ ISC in the statistical limit which corresponds to a small electronic energy gap.[73]

The intramolecular dynamics in the S_1 manifold of anthracene and its derivatives exhibits mode specificity of ISC due to the interplay between two classes of effects. First, intrastate coupling, which corresponds to the intermediate level structure in S_1, and second, resonance effects due to interstate coupling of S_1 states with a relatively sparse $\{T_x^k\}$ manifold. These mode-specific effects will prevail only provided that either the $\{S_1\}$ manifold or the $\{T_x^k\}$ manifold is sparse. Such effects are expected to be exhibited only in the low energy region (A) and in the intermediate energy region (B). In the high E_v domain all vibrational mode specificity for ISC disappears due to efficient IVR in the S_1 manifold, while all resonance effects are cancelled out in the statistical mediating $\{T_x\}$ manifold. Intramolecular ISC in this high-energy domain corresponds to "chemical"-type intramolecular dynamics in an isolated molecule where all mode-specificity effects are eroded.

TABLE VII. High E_v ISC rates of anthracene derivatives.

Molecule	E_v (cm^{-1})	Y	$k_{nr}\tau_{rad}$
Anthracene	2919	0.132	6.6
Anthracene-D_{10}	2893	0.130	6.7
9CN Anthracene	2718	0.13	6.7
9,10-dichloroanthracene	8271	0.017 1	58
9-bromoanthracene	1770	0.001 24	806
9,10-dibromoanthracene	2860	0.001 8	550

ACKNOWLEDGMENTS

We are greatly indebted to Dr. C. Cossart for collaboration on the numerical calculations of the rotational contours of anthracene reported in Sec. III A. We are grateful to Professor A. H. Zewail for communicating to us his anthracene lifetime data, for prepublication information, and for interesting discussions. We are indebted to Professor E. C. Lim for stimulating discussions and comments. We wish to thank Mark Sonnenschein for his assistance in the experimental work and in data handling. This research was supported by the United States Army through its European Research Office (to J. J.) and by the Fund for Basic Research of the Israel Academy of Sciences (to A. A.)

[1] H. Von Weyssenhoff and E. W. Schlag, J. Chem. Phys. **51**, 2508 (1968).
[2] C. S. Parmenter and M. W. Schuyler, Chem. Phys. Lett. **6**, 339 (1970).
[3] K. G. Spears and S. A. Rice, J. Chem. Phys. **55**, 5561 (1971).
[4] J. C. Hsieh, C. S. Huang, and E. C. Lim, J. Chem. Phys. **60**, 4345 (1974).
[5] D. H. Levy, Annu. Rev. Phys. Chem. **31**, 197 (1980).

[6]A. Amirav, U. Even, and J. Jortner, J. Chem. Phys. **71**, 2319 (1979).
[7]F. M. Behlem, N. Mikami, and S. A. Rice, Chem. Phys. Lett. **60**, 364 (1979).
[8]A. Amirav, U. Even, and J. Jortner, J. Chem. Phys. **75**, 3770 (1981).
[9]U. Even and J. Jortner, J. Chem. Phys. **77**, 4391 (1982).
[10]W. R. Lambert, P. M. Felker, and A. H. Zewail, J. Chem. Phys. **75**, 5958 (1981).
[11]P. M. Felker, W. R. Lambert, and A. H. Zewail, Chem. Phys. Lett. **89**, 309 (1982).
[12]P. M . Felker and A. H. Zewail, Chem. Phys. Lett. **102**, 113 (1983).
[13]A. Syage, W. R. Lambert, P. M. Felker, A. H. Zewail, and R. M. Hochstrasser, Chem. Phys. Lett. **88**, 266 (1982).
[14]P. M. Felker, W. R. Lambert, and A. H. Zewail, J. Chem. Phys. **77**, 1603 (1982).
[15]P. M. Felker, J. A. Syage, W. R. Lambert, and A. H. Zewail, Chem. Phys. Lett. **99**, 1 (1982).
[16]P. M. Felker and A. H. Zewail, Chem. Phys. Lett. **94**, 448, 454 (1983); J. Chem. Phys. **78**, 5266 (1983).
[17]W. R. Lambert, P. M. Felker, and A. H. Zewail, J. Chem. Phys. **81**, 2217 (1984).
[18]W. R. Lambert, P. M. Felker, J. A. Syage, and A. H. Zewail, J. Chem. Phys. **81**, 2195 (1984).
[19]J. A. Syage, P. M. Felker, and A. H. Zewail, J. Chem. Phys. **81**, 2209 (1984).
[20]T. Majors, U. Even, and J. Jortner, J. Chem. Phys. **81**, 2330 (1984).
[21]K. Rademann, U. Even, S. Rozen, and J. Jortner, Chem. Phys. Lett. **125**, 5 (1986).
[22]S. Okajima, B. E. Forch, and E. C. Lim, J. Phys. Chem. **87**, 4571 (1981).
[23]T. R. Hyes, W. Henke, H. Selze, and E. W. Schlag, Chem. Phys. Lett. **77**, 19 (1981).
[24]A. Amirav, U. Even, and J. Jortner, Chem. Phys. Lett. **83**, 1 (1981).
[25]T. Zwier, E. Carrasquillo, and D. H. Levy, Chem. Phys. **78**, 5493 (1983).
[26]A. Amirav and J. Jortner, Chem. Phys. Lett. **94**, 547 (1983), **95**, 295 (1983).
[27]M. Sonnenschein, A. Amirav, and J. Jortner, J. Phys. Chem. **88**, 4217 (1984).
[28]A. Amirav, M. Sonnenschein, and J. Jortner, Chem. Phys. Lett. **100**, 488 (1983).
[29]A. Amirav and J. Jortner, J. Chem. Phys. **84**, 1500 (1986).
[30]A. Amirav, M. Sonnenschein, and J. Jortner, Chem. Phys. **102**, 305 (1986).
[31]We have measured the vibrational energy dependence of the absolute quantum yield in the S_1 manifold of tetracene, perylene, fluorene, carbozole, indole, transstilbene, and 4-Cl transstilbene. A Amirav and J. Jortner (unpublished).
[32]R. E. Kellog, J. Chem. Phys. **44**, 411 (1966).
[33]R. G. Bennet and P. J. McCartin, J. Chem. Phys. **44**, 1969 (1966).
[34]W. R. Ware and B. A. Baldwin, J. Chem. Phys. **43**, 1194 (1965).
[35]E. C. Lim, J. D. LeDosa, and J. M. Yu. J. Mol. Spectrosc. **19**, 412 (1966).
[36]M. Bixon and J. Jortner, J. Chem. Phys. **48**, 715 (1968).
[37]J. P. Roberts and R. S. Dixon, J. Phys. Chem. **75**, 845 (1971).
[38]Y. H. Meyer, R. Astier, and J. M. Leclerq, J. Chem. Phys. **56**, 801 (1972).
[39]A. Kearbell and F. Wilkinson, J. Chim. Phys. **20**, 125 (1970).
[40]T. F. Hunter and R. F. Wyatt, Chem. Phys. Lett. **6**, 221 (1970).
[41]R. P. Widman and J. R. Huker, J. Phys. Chem. **76**, 1524 (1972).
[42]G. D. Gillespie and E. C. Lim, J. Chem. Phys. **65**, 2202 (1976).
[43]G. D. Gillespie and E. C. Lim, Chem. Phys. Lett. **63**, 355 (1979).
[44]K. C. Wu and W. R. Ware, J. Am. Chem. Soc. **101**, 5906 (1979).
[45]K. Hamanouse, S. Hirayama, T. Nakayama, and H. Teranishi, J. Phys. Chem. **84**, 2074 (1980).
[46]M. Tanaka, I. Tanaka, S. Tai, K. Hamanouse, M. Sultani, and K. Yoshihara, J. Phys. Chem. **87**, 813 (1983).
[47](a) A. Amirav, U. Even, and J. Jortner, J. Chem. Phys. **75**, 2489 (1981); (b) S. Leutwyler, Chem. Phys. Lett. **107**, 284 (1984).
[48]A. Amirav and J. Jortner, Chem. Phys. Lett. **132**, 335 (1986).
[49]G. Beck, Rev. Sci. Instrum. **45**, 318 (1974).
[50]R. Parish, J. Chem. Phys. **24**, 250 (1956); **25**, 1112 (1956).
[51]A. J. McHugh and I. G. Ross, Spectroschim. Acta **24A**, 441 (1970).
[52]F. W. Birss, S. D. Colson, and D. A. Ramsay, Can. J. Phys. **51**, 1031 (1973).
[53]F. A. Novak and S. A. Rice, J. Chem. Phys. **71**, 4680 (1979); **73**, 858 (1980).
[54](a) E. Riedle and H. J. Neusser, J. Chem. Phys. **80**, 4686 (1984); (b) E. Riedle, H. J. Neusser, and E. W. Schlag, J. Phys. Chem. **86**, 4877 (1982).
[55](a) A. Amirav, J. Jortner, S. Okajima, and E. C. Lim, Chem. Phys. Lett. **126**, 487 (1986); (b) A. Amirav, J. Jortner, M. Terazima, and E. C. Lim, *ibid.* **133**, 179 (1987).
[56](a) B. E. Forch, K. T. Chen, H. Saigusa, and E. C. Lim, J. Phys. Chem. **87**, 2280 (1983); (b) B. E. Forch and E. C. Lim, Chem. Phys. Lett. **110**, 593 (1984); (c) A. Amirav, J. Chem. Phys. **86**, 4607 (1987).
[57]A. Amirav, Chem. Phys. **108**, 403 (1986).
[58]W. E. Henke, W. Yu, H. L. Selzle, E. W. Schlag, D. Wutz, and S. H. Lin, Chem. Phys. **92**, 187 (1985).
[59]N. Liver, A. Nitzan, A. Amirav, and J. Jortner (to be published) J. Chem. Phys. (in press).
[60]Y. Hirata and E. C. Lim, J. Chem. Phys. **69**, 3292 (1978).
[61](a) N. Neto, M. Scrocco, and S. Califano, Spectrochim. Acta **22**, 1981 (1966); (b) K. Ohno, J. Mol. Spectrosc. **77**, 329 (1979).
[62]J. Murakami, M. Ito, and K. Kaya, Chem. Phys. Lett. **80**, 203 (1981).
[63]A. Amirav, U. Even, and J. Jortner, Anal. Chem. **54**, 1666 (1982).
[64]A. Amirav, J. Jortner, S. Okajima, and E. C. Lim, Chem. Phys. Lett. **126**, 487 (1986).
[65]P. M. Felker and A. H. Zewail, J. Chem. Phys. **82**, 2961 (1985).
[66]P. M. Felker and A. H. Zewail, J. Chem. Phys. **82**, 2975 (1985).
[67]P. M. Felker and A. H. Zewail, J. Chem. Phys. **82**, 2994 (1985).
[68]D. P. Craig and G. J. Small, J. Chem. Phys. **50**, 3827 (1969).
[69]J. A. Warren, J. M. Hayes, and G. J. Small, Chem. Phys. **102**, 323 (1986).
[70]F. Duschinsky, Acta Phys. **7**, 551 (1937).
[71]J. A. Warren, J. M. Hayes, and G. J. Small, Chem. Phys. **102**, 313 (1986).
[72]U. Even, A. Amirav, S. Leutwyler, M. J. Ondrechen, Z. Berkovitch-Yellin, and J. Jortner, Faraday Discuss. Chem. Soc. **73**, 153 (1982).
[73]R. Englman and J. Jortner, Mol. Phys. **18**, 145 (1970).